Lawrence Berkeley National Laboratory
LBL Publications

Title

Advanced Monitoring Technology Report For an Integrated Risk Management and Decision-Support System (IRMDSS) for Assuring the Integrity of Underground Natural Gas Storage Infrastructure in California

Permalink

https://escholarship.org/uc/item/2259n8zn

Authors

Zhang, Yingqi

Rodriguez Tribaldos, Veronica

Vasco, Donald

<u>et al.</u>

Publication Date

2024-09-09

Copyright Information

Peer reviewed

Advanced Monitoring Technology Report

For an Integrated Risk Management and Decision-Support System (IRMDSS) for Assuring the Integrity of Underground Natural Gas Storage Infrastructure in California

PREPARED BY:

Primary Author(s):

Yingqi Zhang, Veronica Rodriguez Tribaldos, Donald W. Vasco, Barry M. Freifeld, William Foxall, Kang Wang, Roland Burgmann, Brian Leen, Doug S. Baer and Curtis M. Oldenburg

Lawrence Berkeley National Laboratory
One Cyclotron Road, Berkeley 94720
510 486 4000
https://www.lbl.gov

September, 2021

ACKNOWLEDGEMENTS

ABSTRACT

Previous studies have shown that underground natural gas storage (UGS) in California has served a critical role in meeting energy demands in California, and there is no immediate alternative. Therefore, it is important to ensure the safety of UGS infrastructure, especially considering that many of the UGS sites are using a combination of new and old wells, some of which were installed decades ago and re-purposed for UGS. The purpose of this project is to develop an integrated risk management and decision support system (IRMDSS) to manage risks associated with this heterogeneous subsurface infrastructure.

The approach of the IRMDSS is to take advantage of the predictive capability of mechanistic models, with support from data acquired from advanced monitoring technologies, for evaluation and analysis of various incident scenarios or potential threats. In this project, we have demonstrated data collection by four advanced monitoring technologies. These include two downhole monitoring technologies, distributed temperature sensing (DTS), distributed acoustic sensing (DAS), and two surface monitoring technologies, Interferometric Synthetic Aperture Radar (InSAR), and unmanned aerial vehicle (UAV). DTS and DAS data are collected continuously, providing information related to individual wells. InSAR data are collected frequently (~every 24 days), and UAV data can be collected as frequently as is practical depending on need. Together, these subsurface and surface monitoring technologies provide near real-time information useful for risk management of UGS facilities.

TABLE OF CONTENTS

LIST OF FIGURES

LIST OF TABLES

EXECUTIVE SUMMARY

Introduction or Background

The general purpose of underground gas storage (UGS) is to meet varying demand for natural gas (predominantly methane, CH_4) over daily to seasonal time scales. Recent studies show that UGS is likely to remain a requirement for reliably meeting winter peak demand (Conclusion 2.15 of CCST report) in California in the near term. However, there are well-known risks associated with deep underground natural gas storage at high pressure. Broadly speaking, there are two potential failure scenarios related to subsurface containment. One is related to well leakage, where wells are an engineered component of the system. The second broad failure scenario comes from failure of the natural system to contain gas (such as would occur if caprock integrity is compromised resulting in leakage through caprock). Leakage failure scenarios can cause potential damage or catastrophic impacts to natural gas storage facilities. The overall goal of the project is to address these risks by developing an Integrated Risk Management and Decision-Support System (IRMDSS). One specific goal of the IRMDSS is to demonstrate advanced monitoring technologies to help manage UGS risks.

The current standard monitoring programs employed at natural gas storage fields include wellhead pressure and temperature, surface leakage detection, and well-logging and well inspections. Current practice is to monitor wellhead pressure and then compute the corresponding bottomhole (reservoir) pressure using gas thermodynamic models. The problem is that variable or unknown temperature of the column of gas in the wellbore leads to a significant uncertainty in the density of the wellbore fluid which then gets carried over into the estimate of the bottomhole pressure. These uncertain pressure estimates may lead to erroneous estimates of gas inventory, which may mask even moderate leaks. The current regulator-required method for identifying leaks in a gas storage well is to perform annual noise and temperature logs. Thermal anomalies from temperature logs can be indicative of subsurface flow. Temperature logs were obtained for all wells in the field in 2016, as required by the California Division of Oil, Gas, and Geothermal Resources (DOGGR), now known as CalGEM. Noise logs can also be used to identify anomalous flow, as high-pressure gas will create a detectable acoustic signature. While annual noise and temperature logs can be used to spatially identify wellbore leaks, they cannot indicate if a well failure is imminent, and it is possible for the well to leak the day after an inspection and the leak can grow significantly in severity prior to the next logging run.

This report documents the monitoring effort in the project. A number of advanced monitoring technologies including in-situ and surface monitoring approaches are demonstrated in the IRMDSS as detailed below.

Project Purpose

Many risk management approaches focus on hazard and threat identification using engineering methods and do not fully exploit process models to predict or forecast system failure to support preventive measures. The Integrated Risk Management and Decision Support System (IRMDSS) framework developed in this project aims at taking advantage of the prediction

capability of mechanistic models and dynamic, continuous monitoring data from advanced monitoring technologies. The framework allows interaction between models and data for risk assessment, providing workflows for anomaly detection, analysis, and relevant decision support.

The IRMDSS is designed to help operators identify potential risks and to help evaluate various safe operation and failure scenarios. If incidents have already happened, the tool can be used to analyze what happened and evaluate mitigation measures.

The very specific goals of this project include:

- Develop a set of mechanistic models and analyses to estimate the risk and evaluate mitigation strategies for UGS under various operational and failure scenarios. These include a reservoir model, a geomechanical model, a wellbore model, and geohazard analysis.
- Deploy advanced monitoring technologies and demonstrate how continuously updated monitoring data can be used to analyze scenarios.
- Provide a supervisory interface to integrate system components and help users to follow the workflow of the framework.

The proposed framework is demonstrated at the Honor Rancho site in close collaboration with the project partner, Southern California Gas Company (SoCalGas).

Project Approach

The project team consists of nine team members from the Lawrence Berkeley National Laboratory (LBNL), and two subcontractors: Lettis Consultants International, Inc. (LCI), and University of California, Berkeley (UCB). The LBNL team leads the project and is responsible for the overall framework and most of the modeling and monitoring activities. LCI provides support on geohazard analysis. UC Berkeley provides support on obtaining and pre-processing InSAR data. The project partner is SoCalGas, owner and operator of the Honor Rancho UGS facility which serves as the test site for data collection and framework development and testing.

The IRMDSS framework being developed in this project includes three components: models; advanced monitoring technology; and use cases that provide workflow/examples for pre-defined scenarios. Key activities of the project include:

1. Development of site-specific applications of models of key processes such as geomechanical deformation, reservoir flow, wellbore flow, and geotechnical hazards (documented in the project 2nd annual report).
2. Deploy advanced monitoring technologies:
   - Downhole quartz pressure/temperature sensors, which provide real-time measurements of pressure and temperature at the bottom of the instrumented well. (These direct downhole measurements avoid the potential uncertainties arising from the current practice of estimating downhole conditions using wellhead measurements.)
   - Fiber-optic Distributed Temperature Sensing (DTS), which provides a continuous temperature measurement along the wellbore. This profile could be different between normal and abnormal conditions, and therefore such data can be very useful in leakage detection and analysis.

- Fiber-optic Distributed Acoustic Sensing (DAS), which is a technology that can quickly detect and locate the acoustic signal generated by a gas leak in a well.
- Unmanned Aerial System (UAS)/Drone Gas leak monitoring, which is used to monitor CH_4 atmospheric concentrations at ground surface for surface leakage detection.
- Interferometric Synthetic Aperture Radar (InSAR) for ground deformation, which measures millimeter-scale changes in surface deformation over spans of days to years. The surface deformation can then be transformed to infer the volume changes within the reservoir associated with pressure changes due to natural gas storage operations.

Both analytical models and monitoring data are integrated in the IRMDSS framework through use cases. A use case is a written description of the use of a system, specifically here a list of actions or steps that should be taken to achieve a defined goal with the IRMDSS. The IRMDSS framework and related use cases are based on the operations, properties, and conditions of the SoCalGas Honor Rancho UGS site.

This monitoring report only includes efforts in demonstrating advanced monitoring technologies; other parts of the IRMDSS project are summarized in other task-specific reports.

Technology/Knowledge Transfer/Market Adoption (Advancing the Research to Market)

The goal of technology/knowledge/market transfer is to communicate the methods, technologies, and learnings developed and derived from this project with the public, public agencies, and targeted users including UGS utilities and stakeholders. The communication can be done though written documents, websites, and meetings.

So far, we have prepared reports, presentation material, and a manuscript for publication. We are working on a project website to provide easy access for interested parties. We have held meetings with two utility companies: SoCalGas and PG&E. We will continue all these efforts in the coming year.

Benefits to California

Because the IRMDSS provides an effective risk management framework, it better enables California to continue using UGS for winter energy supply, therefore, the IRMDSS indirectly supports the reliability of energy supply for ratepayers in California. Other expected related benefits include lower costs through better decision-making, increased safety and less loss of life and property, and overall lower risk related to loss of containment as elaborated on below:

- Lower costs: The quantitative predictive methodology developed by the proposed project will enable change of operations or early preventive engineering measures to prevent failure or damage, thus (1) lowering mitigation costs; and (2) lowering potential decrease in deliverability.
- Greater reliability: The science-based risk models combined with re-assessing of risks based on new data provide a risk management system for improving reliability of UGS.
- Increased safety: Identification of precursors to failure or imminent failure likelihood promotes preventive measures that will help to minimize potential negative impacts of methane leaks on human health and safety from catastrophic events. Adoption of new monitoring technologies can improve overall storage security.

- Economic development: In addition to the potential need to match energy storage capacity with increasing saturation of renewable energy sources, improving gas storage integrity can lead to economic development through the need for capital improvements to infrastructure and related labor expenditures.
- Environmental benefits: Early prevention by detection of imminent failures will minimize natural gas leaks and hence reduce emissions of methane, a potent greenhouse gas.
- Public health: Prevention of catastrophic events will protect the public from exposure to reservoir gases and odorants.
- Consumer appeal: Increasing storage integrity and natural gas storage safety in general will enhance the public's trust of utilities and the energy industry in general, allowing for greater public support of upgrades and expansion of energy infrastructure.
- Energy security: By preventing gas leakage and catastrophic events, the system can prevent potential disruptions to deliverability.

The IRMDSS framework can be adopted by each gas company for their individual facility. However, process models are site-specific (i.e., each model is built based on each site's geological conditions), therefore, new model inputs need to be constructed when a new site adopts the method. The general framework can still be applied.

The money that could be saved is hard to estimate for a technology aimed at risk reduction through prevention. However, incidents involving loss of well control can result in significant costs. If preventive measures are available, or some effective modeling tools can be applied to find effective mitigation strategies, then there is the potential for huge financial savings.

CHAPTER 1:
Introduction

Project Background

Underground natural gas storage (UGS) utilizes various underground units including depleted gas/oil reservoirs, aquifers, or salt caverns to store natural gas delivered by transmission pipelines (from long distances, often from out of state) near demand centers for use during periods (typically cold spells in winter) when demand exceeds pipeline deliverability. The general purpose of UGS is to meet varying energy demands at different times, with time scale changing from daily to seasonal. Based on a recent CCST report (2018) Conclusion 2.15, UGS is likely to remain a requirement for reliably meeting winter peak demand in California in the near term. Given there is no immediate alternative other than UGS to provide for California's demand for natural gas during peak periods in winter, it is important to ensure the safety of UGS infrastructure. There are well-known risks associated with deep underground natural gas storage at high pressure. Two potential failure scenarios exist related to subsurface containment. One is related to the engineered system, i.e., leakage due to compromised well integrity. Considering that many of the UGS sites are using a combination of new and old wells, some of which were installed decades ago and re-purposed for UGS, well integrity is a major concern regarding safety of UGS. The second broad failure scenario comes from failure of the natural system to contain gas. Such a failure could also cause potential damage or catastrophic impacts to natural gas storage facilities. The overall goal of the project is to address these risks by developing an Integrated Risk Management and Decision-Support System (IRMDSS).

This project aims at developing a framework to provide leading indicators of potential threats by merging advanced models with continuous reevaluation based on data from advanced monitoring techniques. The specific tasks of the project include:

- Develop a set of analytical tools/mechanistic models
    - To evaluate operations and potential impacts of failure scenarios
    - To evaluate impact mitigation strategies
- Demonstrate advanced monitoring technologies
- Provide a supervisory interface for users to apply the developed analytical tools and analyze acquired monitoring data
- Apply the proposed framework to the Honor Rancho Gas Storage Facility in close collaboration with our project partner, Southern California Gas Company (SoCalGas)

This project started in February 2018. The detailed project background including the current status of UGS in California, potential risks related to UGS, current status of risk management, project objectives, and anticipated benefits are all documented in the first Annual Report (Zhang et. al., 2019). The models developed in this project are documented in the second Annual Report of the project (Zhang et. al., 2020). The existing site characterization data and operational data for the demonstration site Honor Rancho are documented in the Data Report

(Zhang et. al., 2019). Without repeating the project background, this report will focus on the advanced monitoring technologies deployed in the project and data collected.

Monitoring Technologies

The current standard monitoring programs employed at natural gas storage fields include wellhead pressure and temperature, surface leakage detection, and well-logging and well inspections. Current practice is to monitor wellhead pressure and then compute the corresponding bottomhole (reservoir) pressure using gas thermodynamic models. The problem is that variable or unknown temperature of the column of gas in the wellbore leads to a significant uncertainty in the density of the wellbore fluid which then gets carried over into the estimate of the bottomhole pressure. These uncertain pressure estimates may lead to erroneous estimates of gas inventory, which may mask even moderate leaks. The current regulator-required method for testing for and/or locating leakage in a gas storage well is to perform annual noise and temperature logs. Noise logs can be used to identify anomalous flow, as high pressure gas will create a detectable acoustic signature, while decompression of gas during leakage can cause anomalous temperatures. Temperature logs were obtained for all wells in the Honor Rancho UGS field in 2016, as required by the California Division of Oil, Gas, and Geothermal Resources (DOGGR). While annual noise and temperature logs can be used to spatially identify wellbore leaks, they cannot indicate if a well failure is imminent, and it is possible for the well to leak the day after an inspection and the leak can grow significantly in severity prior to the next logging run.

The monitoring technologies planned for this project include:

- Downhole quartz pressure-temperature sensors, which provide pressure and temperature real-time measurements at the bottom of the instrumented well. These measurements are much more accurate than estimates made using wellhead measurements, which is the current practice.
- Fiber-optic Distributed Temperature Sensing (DTS), which will provide a continuous temperature measurement along the vertical wellbore. This profile could be different between normal and abnormal conditions, and therefore such data can be very useful in leakage detection and analysis.
- Fiber-optic Distributed Acoustic Sensing (DAS), which is a technology that can quickly detect and locate the acoustic signal generated by a gas leak in a well.
- Unmanned Aerial System (UAS)/Drone Gas leak monitoring, which is used to monitor CH_4 atmospheric concentrations at ground surface for surface leakage detection.
- Interferometric Synthetic Aperture Radar (InSAR) for ground deformation, which measures millimeter-scale changes in surface deformation over spans of days to years. The surface deformation can then be transformed to infer the volume changes within the reservoir associated with pressure changes due to natural gas storage operations.

The WEZU C2 B well (API 0403721475) the Honor Rancho UGS site was identified for deploying downhole monitoring technologies, which include downhole quartz pressure-temperature sensors, DTS and DAS. Southern California Gas reconditioned WEZU C2 B in the fall of 2019, with a new 7" L-80 26# liner hung in the existing 9-5/8" production casing. The sensors and

fiber optic cables were attached to the 3-1/2" tubing string which was installed September 2019. Unfortunately, for unknown reasons the downhole quartz pressure-temperature sensors were never able to acquire data. DTS data on the other hand have been collected continuously since November 2019. DAS data have been collected since February 2020.

InSAR data have been collected from two sources. The analysis and the comparison of the two sets of data, as well as the comparison with the data from the global positioning system (GPS), are documented in this report.

Due to Covid-related site restrictions, the planned UAS drone survey at the Honor Rancho site could not be performed during the project period. Instead, an analogue site with a known leak source in Solano County, CA was used for monitoring demonstration purposes. ABB performed the survey at the site.

CHAPTER 2:
DTS Monitoring

Introduction

The temperature along the length of a well is a fundamental diagnostic parameter that can be used to assess well integrity issues. When a well is under shut-in conditions, the vertical temperature profile of a well follows the natural geothermal gradient once it reaches the thermal-equilibrium state. This vertical temperature profile will change when there are injection/withdrawal activities. In addition, if there is leakage along the well, the temperature may depart from the normal trend depending on the leakage rate. Therefore, thermal logging has long been used for well leakage detection, not only for natural gas storage (Arthur, 2016) but also for other underground injection activities (Zeng et. al. 2012).

The current regulator-required method for identifying leaks (DOGGR Requirements for California Underground Gas Storage Projects, §1726.6) in a gas storage well is to perform annual noise and temperature logs. Given that a leak can be initiated at any time in the life of a well, annual thermal logging may give an incipient casing integrity issue time to grow more serious in the time between logging runs. Increasing the well logging frequency may not be a solution because the logging intervention increases other risks associated with shutting in the well and installing pressure control equipment to facilitate logging.

Distributed temperature sensing (DTS) comprises optoelectronic devices which measure temperatures by means of optical fibers. Temperatures are recorded along the optical sensor cable, thereby forming as a continuous temperature profile. A DTS interrogator is the size of standard personal computer and the sensing cable can measure along an optical fiber up to several kilometers in length. DTS temperature resolution is about 0.02 °C for a 1-hour integration time, or 0.1°C for 5 minutes integration time. Spatial resolution can be as high as 25 cm. The main advantage of DTS is that it can provide temperature profiles 24/7 and be set to alarm on changing conditions.

DTS has been used for other well integrity monitoring applications, specifically geologic storage of CO_2, for detecting leakage in injection wells (Zhang et al., 2018). A notable difference between leakage through injection wells and other leaky wells (abandoned or monitoring wells) is that the thermal signature of an injection well will be dominated by the flowing liquid in the well. In addition, depending on where the leakage occurs and leakage size, injection fluid temperature as well as pressure drop could have an influence on the temperature signal.

Zhang et al. (2018) simulated temperature profiles along a well with a CO_2 leak occurring during fluid injection, as shown in Figure 2-1. The injection temperature profiles displayed occur both during and after CO_2 injection. The dashed-dot lines are from a scenario where the well has a bad cement job and CO_2 enters the formation at about 1920 m depth. The profiles show an obvious temperature deviation from the expected trend. Although these results are simulation results, other field measurements have shown similar abnormal profiles due to leakage.

Figure 2-1. A temperature profile for an injection well under normal and leakage conditions
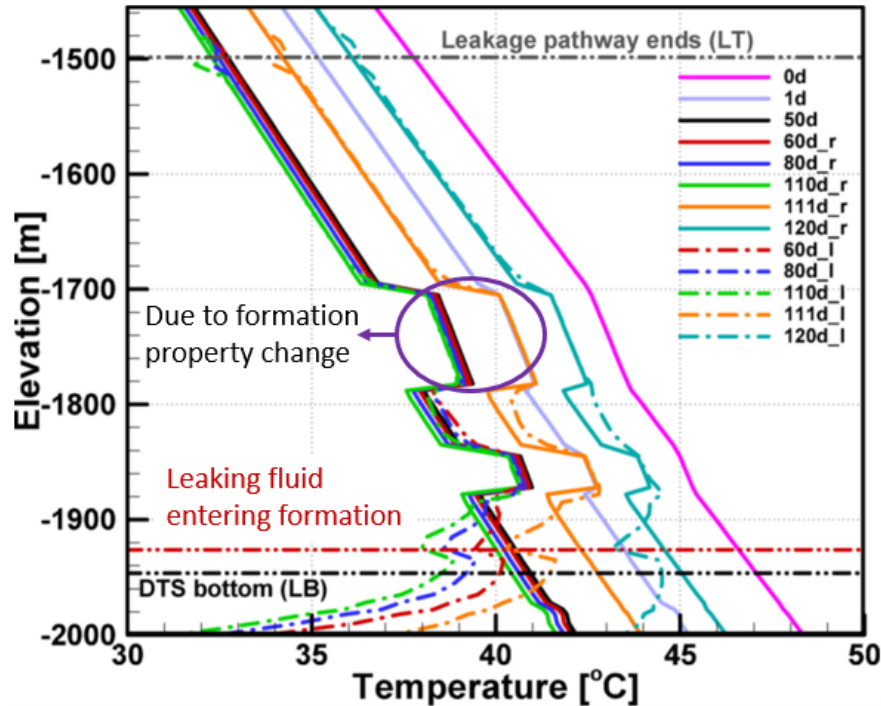
The temperature profiles at different times are indicated by different colors, i.e., 0d means at time 0 days, when the injection is about to begin, 1d means a day after injection and so on. Solid lines are results under normal conditions and dashed-dot lines are results from a leakage scenario (Zhang et al., 2018).

In short, temperature anomalies may indicate integrity issues. To locate leakage location(s) and quantify leakage size, other analyses (e.g., wellbore modeling) may be needed.

Field Instrumentation

The workover for the project well WEZU C2B was conducted in September 2019. The downhole control line was strapped onto the tubing string using Cannon Services joint protectors, to a total depth of 8,418 ft (ftKB), landing near the production packer which was set at 8,432 ft (ftKB). Figure 2-2 shows the rack-mount cabinet, which is a NEMA 4 enclosure. From top to bottom in the rack are a computer monitor, our LINUX server with data storage array, XT-DTS temperature-sensing unit, and the iDAS acoustic-sensing unit. The black tubes are for the air conditioning unit located on the back corner of the slab. The gray junction boxes are for power supply to both the A/C unit and the electronics in the cabinet.

Figure 2-2. Picture of instrumentation rack

Figure 2-3 shows the conceptual layout for the network connectivity that is used for passing data within the data acquisition system.

Figure 2-3. Conceptual layout for the data acquisition unit
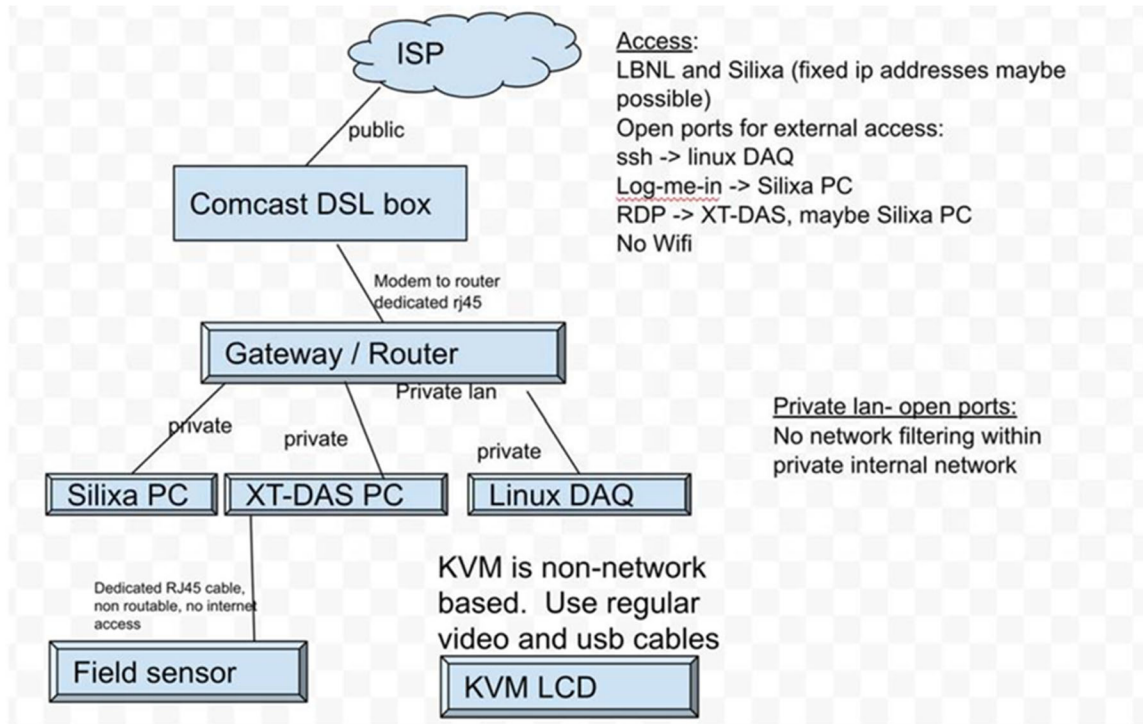
Figure 2-4 shows the design for the control line to operate the downhole pressure-temperature gage and to acquire DTS and DAS data. Figure 2-5 shows the wellhead with the cable installed downhole (attached to the tubing wall). Eventually the cable was attached to the interrogator units.

Figure 2-4. Design of the downhole hybrid fiber-optic copper conductor cable

TWO CONDUCTORS AND FOUR FIBERS in a STAINLESS STEEL TUBE NO JACKET
20,000 PSI SYSTEM

- METAL SHEATH
- FILLER BELT
- COPPER CONDUCTOR
- CENTRAL STRENGTH MEMBER (OPTIONAL)
- BUFFER TUBE & FIBERS
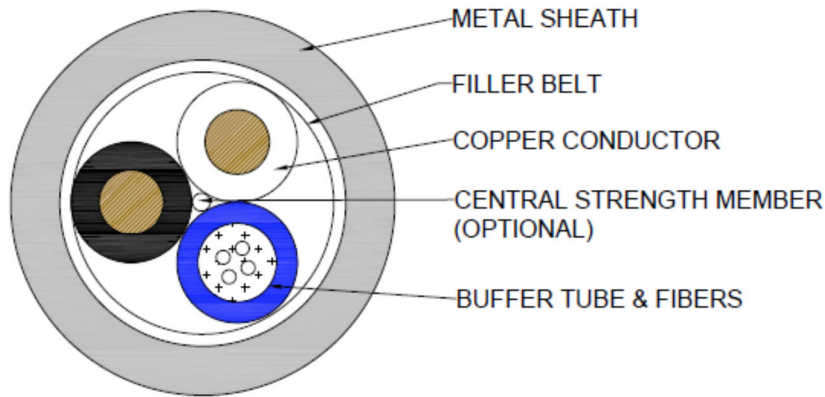
OPTICAL FIBER 50/125 (#1-#2)	Draka 50/125 High Temperature 150°C Acrylate Coated Fibers
OPTICAL FIBER SMF (#3-#4)	Draka Bendbright^XS Single Mode High Temperature 150°C Acrylate Coated Fibers
BUFFER TUBE (#1)	ECTFE oversized tube containing four (4) optical fibers and hydrogen scavenger gel. O.D.: 1.83 mm (0.072") I.D.: 1.32 mm (0.052")
CONDUCTOR	18 AWG 7/26 2% Nickel Coated Copper O.D.: 1.22 mm (0.048")
CONDUCTOR INSULATION	Colored FEP O.D.: 1.8 mm (0.070")
CENTRAL STRENGTH MEMBER (Optional)	Epoxy Fiberglass Rod

Design of the downhole hybrid fiber-optic copper conductor cable. The copper lines are used to operate the downhole pressure-temperature gage, and the fiber-optic lines acquire DAS and DTS data.

Figure 2-5. Picture Showing the Hydrbid cable in Figure 2-4 connected to the wellhead

Data Acquisition and Analysis

DTS data have been collected continuously since November 2019. The temperature profile is recorded about every 10 minutes, amounting to ~144 profiles per day. The temperature profiles are text-based files that can be open by any standard text editor. The downhole cable length is about 2500 m, samples are taken every 25cm (i.e., a total of 10,000 data points per profile), leading to a file size on the order of 500 KB per file. DAS data sampling frequency was set at 1kHz. Spatial sampling was 0.25 m initially, increased to 1 m later to reduce the total amount of data.).

The project well is located within the gas cap and is primarily used for gas injection. As a result, the majority of data are collected during shut-in periods, or during gas injection. However, based on personal communication with SoCalGas, we learned that this well was occasionally used for withdrawal in December 2019. Therefore, we are able to present the DTS temperature profile during a withdrawal period, in addition to a typical profile during gas injection. We selected Feb 22 to24, 2020 DTS data as an example dataset, as it overlapped with DAS data that has been analyzed for acoustic properties.

The data presented here are after both depth correction (removal of cable length that lies above the ground surface) and temperature correction (calibrated based on the temperature log data from 12/20/2019 as shown in Figure 2-6). Time shown is in GMT (local standard time +7 hours).

Temperature profile during withdrawal

Figure 2-7 shows well temperature changes over a two-day period, December 28-29, 2019. Most of the time the well was under shut-in condition, with the temperature following the natural formation geothermal gradient. Gas injection started between hour 15-16 on the first day and ended after the beginning of the second day. Compared to the temperature during shut-in period, the figure shows a temperature drop at the bottom of the well (compared to the temperature during shut-in period), and temperature increase at the top of the well.

During gas withdrawal, the well temperature is affected by a number of factors: the temperature of gas in the reservoir, and the Joule Thomson effect cooling due to gas expansion. In order to understand and interpret the DTS data over time, we used one of the model components of the IRMDSS, namely T2Well, to simulate wellbore temperatures over time. Initial simulations using T2Well indicated that cooling caused by gas expansion alone near the bottom of the well was a minor effect. T2Well simulations showed that not much cooling is occurred at the well bottom if the gas temperature in the reservoir is assumed the same as the formation temperature calculated using the formation geothermal gradient.

Figure 2-6. Temperature survey of the WEZU C2B well

TEMPERATURE SURVEY	
OPERATOR	Southern California Gas Co.
FIELD	Honor Rancho
WELL	WEZU C2B
API NUMBER	0403721475-00
SURVEY DATE	12/20/2019
SHUT IN DATE	12/19/2019
FIELD PRESSURE, PSIA	3147.0
FIELD INVENTORY, BCF	23.40
TBG PRESSURE, PSIA	3183.0
CSG PRESSURE, PSIA	39.0
MAX RECORDED TEMP	185F @ 8921'
EFFECTIVE DEPTH, FT	9219
LOGGED DEPTH, FT	9216
LOGGING SPEED, FPM	30
GAUGE ID	503
ENGINEER	J.Magana
WITNESSED BY	G.Mark

The survey data are provided by SoCalGas (personal communication)

15

Figure 2-7. DTS temperature profile on December 28~29, 2019 during a period of gas withdrawal
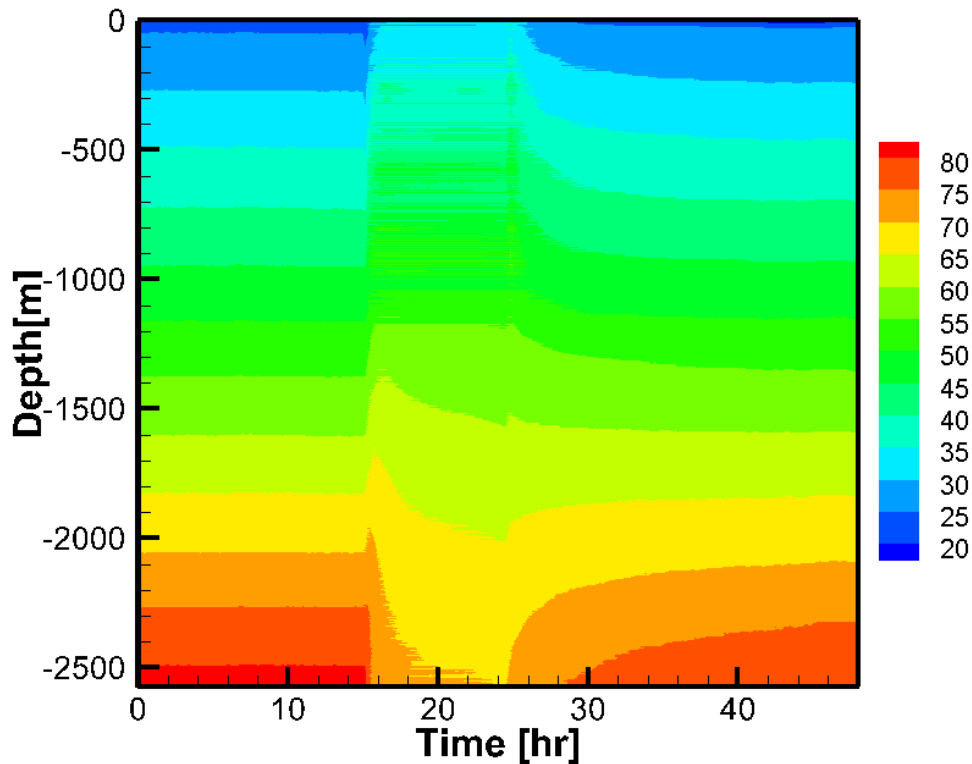
However, the temperature survey (Figure 2-7) provided by SoCalGas on December 20, 2019 indicates the temperature at the reservoir level is about 10 ºC lower than the temperature suggested by the geothermal gradient. To understand how much this may affect the well temperature, we performed additional T2well simulations for this wellbore assuming the gas stored in the reservoir was cooler than the formation at that depth initially. For this simulation we lowered the formation temperature by 10 ºC. The gas withdrawal starts after one hour of shut-in period and lasts for 9 hours. A gas withdrawal rate of 5.5 kg/s is used to obtain a similar wellhead pressure drop (provided by SoCalGas through personal communication) during withdrawal.

The simulated temperature profile is shown in Figure 2-8. As shown, the simulation produces a temperature profile qualitatively similar to the measured one shown in Figure 2-6. The reason that the T2Well simulation is not identical to the DTS data is that the thermal properties of the formation are uncertain so how fast the well changes temperature due to withdrawal and shut-in re-equilibration is uncertain. But the change in temperature trend is the same along the length of the well. As long as the initial measurements are taken and used as baselines and to calibrate mechanistic models such as T2Well, observed deviations from baselines can indicate potential problems, and mechanistic models such as T2Well can be used to evaluate and analyze the potential causes of anomalies such as leakage from tubing or casing.

Figure 2-8. Temperature profiles simulated using T2Well
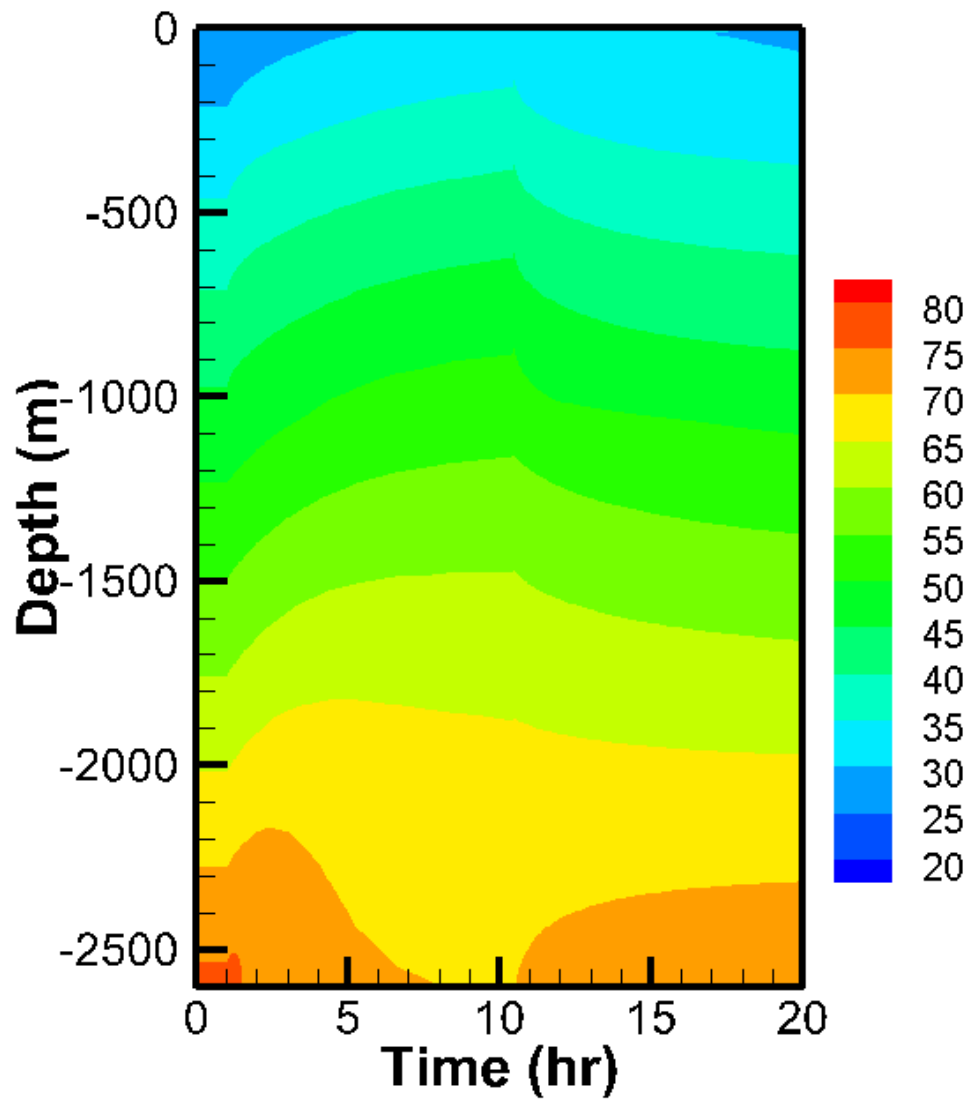
Temperature profile during injection

Temperature profiles during injection follow similar patterns. To be consistent with DAS data analysis, the DTS profile during February 22~24 is presented here.

Figure 2-9. DTS temperature profile on February 22~24
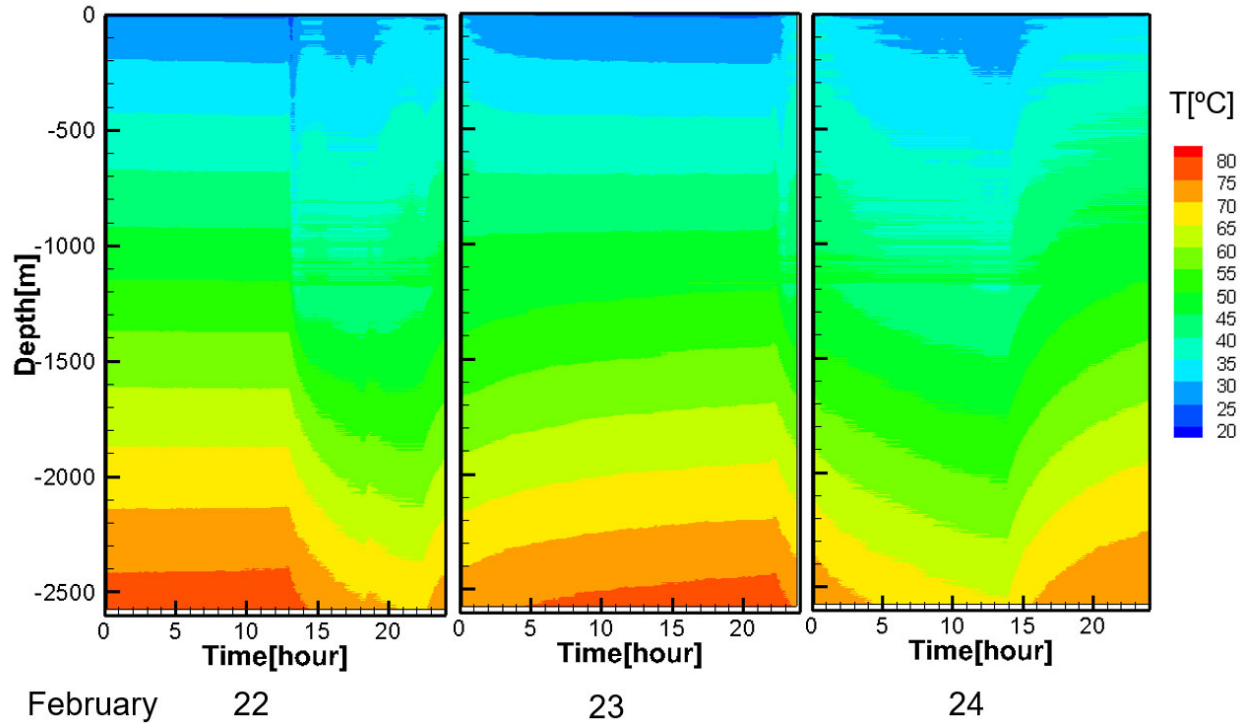
The figure shows initially (at the beginning on February 22nd) the temperature was equilibrated with the formation geothermal gradient. The first injection started on the 13th hour of February 22nd, and lasted for about 10 hours. This is indicated by the cooler temperatures due to the cold gas injection. The temperature profile on the 23rd shows a long recovery from the cold gas injection, then this is followed by another injection, which started at around 10 pm. The temperature starts to cool down again. The injection lasted for about 16 hours. Then the temperature started to recover when the injection stopped.

A distinct feature of these DTS profiles is that the measured temperature shows more noise in the upper part of the profile during operations (injection and withdrawal). This can be seen more clearly by focusing into a single temperature profile, as shown in Figure 2-10. The reason for this increase in "noise" is that the annulus of the well is filled with both gas (upper part) and treated brine (lower part), which is liquid. The treated brine in the annulus is used to stabilize the packer, by providing force to counteract the pressure in the reservoir. Maintenance of the brine height is a critical component of well integrity. The fiber optic cable is clamped to the tubing at discrete points along the tubing, as shown in a picture taken at the field in Figure 2-11. The lower part of the cable is in the brine, which has higher thermal conductivity than the gas in the shallower section of the annulus. While it appears that the oscillations are "noise," in fact the thermal signature reflects that the cable is clamped to the tubing roughly every joint

length, and in between the clamps, the cable sits entirely surrounded by fluid. The DTS cable thus reflects both the tubing temperature (where it is clamped) and the ambient annular fluid temperature through which it runs between clamps. Therefore the DTS cable shows that there is a strong thermal gradient under transient conditions between the inside of the tubing and the annulus and surrounding formation. The oscillations observed are real reflections of the gradient given the very small variations in cable position. The stronger oscillations at shallower depth reflect the lower thermal conductivity of annular gas as compared to the higher thermal conductivity of the liquid-filled annulus below the gas-liquid contact.

Figure 2-10. A DTS profile at one time during withdrawal(left) and injection (right)
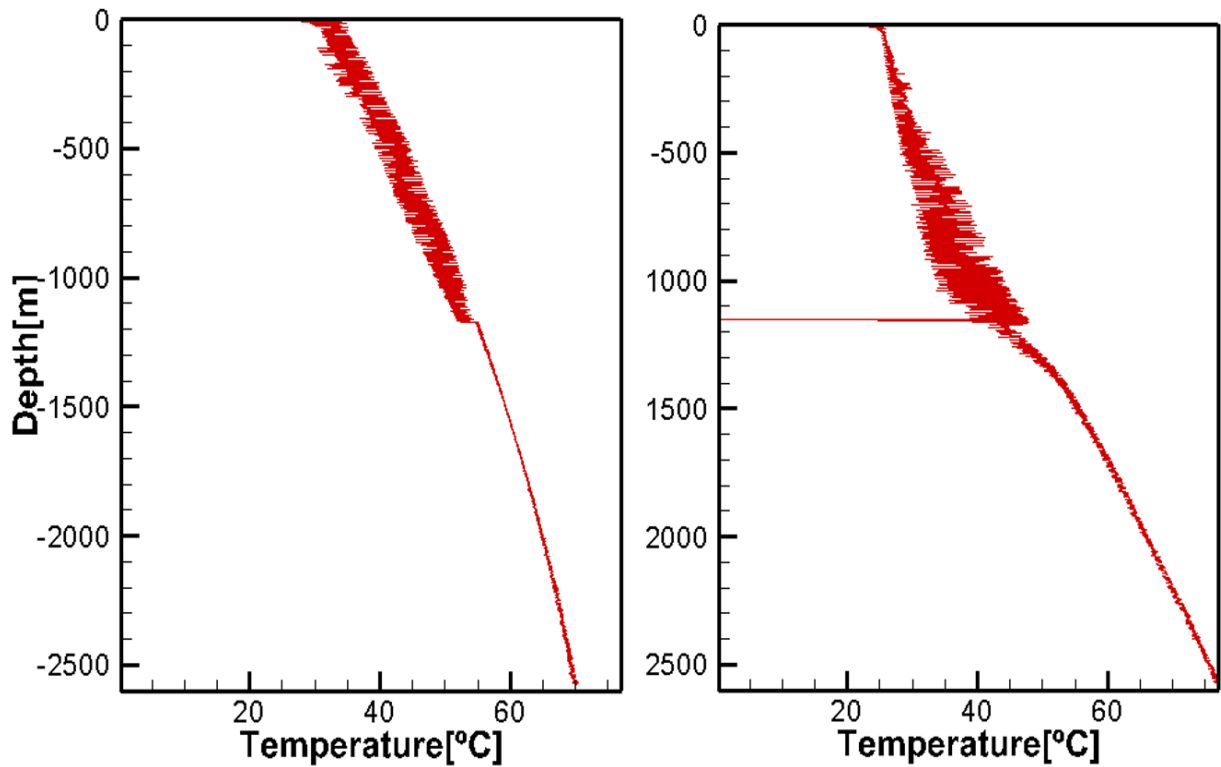
The left figure shows the first temperature measurement on Dec. 29, 2019, when before withdrawal stopped; the right figure is the temperature at hour 13 on Feb. 22, shortly after injection started.

Figure 2-11. Tubing with fiber optic cables clamped in
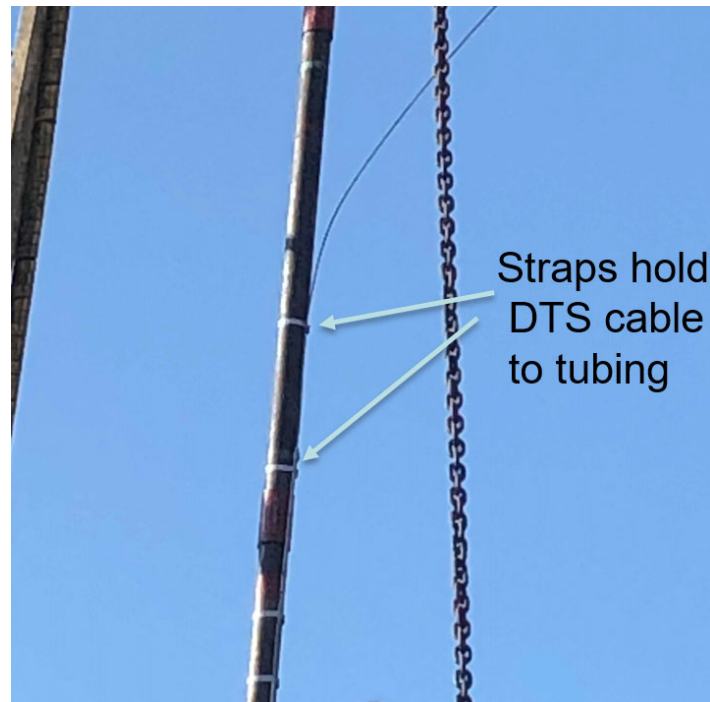
This feature of DTS measurement brings an extra benefit for maintaining well integrity. Figure 2-10 clearly shows that the location of the gas/liquid interface in the annulus is around 1150 m. Knowing the level of gas/liquid contact is important in risk assessment, as an unexpected change of the level could indicate integrity problems. However, current practice is to identify the interface based on the use of a sonic level monitoring system. The sonic measurements are highly inaccurate, and could result in a level determination of ±20 m. In comparison, the DTS measurement provides for continuous monitoring of the annulus fluid level and with an accuracy of ±50 cm. While we showed the thermal variation during a period of gas injection, it is also possible to identify the location of the gas/liquid interface when the well is shut-in, as the thermal variation is always greater in a gas column than in a liquid column. This is caused by natural fluid convection creating small -variations in the temperature profile which are stronger in the gas than liquid.

Summary and Conclusion

In this section, we presented some of the DTS data collected in well WEZU C2 B at the Honor Rancho site. The project well is primarily used as an injection well, although Southern California Gas periodically operates it also for withdrawal. During gas withdrawal, the temperature at the well bottom becomes cooler and the temperature in the upper part of the well becomes warmer. As an example of an IRMDSS workflow, we have performed a simulation using the T2Well model to analyze and explain the observed DTS temperature profile. During gas injection, we see clearly a cooling trend of the DTS profiles, which is expected. All the DTS measurements from injection show similar patterns, which provides a good baseline for integrity issues. In addition, the DTS measurements provide the gas-liquid contact location in the annulus on a regular basis (e.g., whenever the well is operated to produce transient

contrasting temperatures between tubing and annular fluid), which is an important piece of information for identifying integrity issues. We have not seen anomalies since we started to take DTS measurements. However, if that happens, the vertical temperature measurements can be used with a combination of a wellbore model to identify potential leakage locations and quantify leakage size.

CHAPTER 3:
DAS Monitoring

Introduction

One of the key aspects of ensuring the safety of underground natural gas storage (UGS) infrastructure is the ability to continuously monitor its state-of-health and to rapidly identify potential hazards. One way of detecting abnormal and potentially threatening conditions is by analyzing acoustic noise passively generated by fluid or gas flow in the well. Turbulence generated by channelized flow across/through perforations or leakage pathways generates high-amplitude, characteristic acoustic signals that deviate from background noise generated during injection or withdrawal operations, enabling identification of anomalous behavior in the system. The most common technique used to listen to this noise and detect well leaks and other well integrity issues is spectral noise logging (e.g., Maslennikova et al., 2012). This method, used in industry since the 1970's, consists of lowering a noise logging tool down the borehole and recording acoustic noise at different frequency channels, either as a continuous reading along the borehole or as stationary measurements at different depths. Although this technique has been proven successful in leak detection, a major drawback of its application is that this tool cannot be permanently deployed in the well for continuous monitoring. Every time a survey is performed, it requires operators to lower the logging tool down the borehole and to be present for the procedure, which is expensive and time-consuming. Thus, current practice is limited to one noise logging survey per year, which limits the ability to detect leaks or other well-integrity issues before they represent a hazard to the system.

Distributed Acoustic Sensing (DAS) is an attractive alternative to the current approach. This emerging technology converts common fiber-optic cables into arrays of strain-rate sensors that are responsive to vibrations surrounding the cable. A fiber-optic cable is easily deployed down the borehole in a variety of configurations (e.g., behind casing for permanent deployment, strapped to tubing for more temporary acquisitions) and connected to an interferometric device that can continuously record acoustic signals at very high spatial and temporal resolution, providing in-situ, real-time information on the acoustic characteristics of the well. In this way, a continuous record of the noise can be acquired, making DAS a potential tool for long-term monitoring of UGS infrastructure.

In this chapter, we describe our development of a workflow to analyze the continuous acoustic signal generated along the borehole throughout the complete cycle of operations recorded using DAS. By characterizing the acoustic noise generated during normal operations at the UGS, background conditions can be established and a system can be developed to detect anomalies in the acoustic record.

Distributed Acoustic Sensing (DAS)

Distributed Acoustic Sensing (DAS) utilizes a photonic technique called phase-sensitive time-domain reflectometry (Φ-OTDR) to accurately measure strain change along an optical fiber (Hartog et al., 2010). An interrogation unit (IU) sends consecutive laser pulses down a fiber-optic cable connected to the instrument (Figure 3-1a). Natural impurities in the silica core of the fiber result in differences in the refractive index of the core. As a result, part of the light sent down the cable will be backscattered along the fiber at these impurities, and it will be recorded back at the IU. If the fiber-optic cable is strained by, for example, a vibration, the phase of the backscattered light will change between pulses (Figure 3-1b). For the purposes of DAS instruments using Rayleigh backscattering (one specific type of photonic backscattering, the one used in this study), the change in optical phase $\Delta\Phi$ per pulse time τ measured by the IU at each measurement point x depends only on the change in length over a reference length in the cable termed gauge length, x_g, along the axial direction of the fiber, i.e., the change in mechanical strain (contraction or dilation) along the fiber ε_{zz}:

$$\varepsilon_{zz}(\tau, x) = \frac{\Delta x}{xg}(\tau) = C \cdot \Delta\phi$$

where the constant factor C contains information on the phase of the backscattered light, which in turn depends on the refractive index of the fiber core and the wavelength of the laser pulse, and an additional multiplicative factor related to known material properties of the fiber.

$\Delta\Phi$ is measured with respect to the previous laser pulse. Hence, the DAS system measures a record of strain-rate, i.e., the strain accumulated since the previous pulse time, divided by the time between pulses. Measurement points are virtual locations along the fiber commonly referred to as channels, which are the result of averaging backscattering occurring at many closely-spaced (~100 microns) scattering points to deliver a single measurement per channel spacing subject to the gauge length. Channel spacing can be as small as 0.25 m and is defined by the user. Gauge lengths can vary from a few meters to 10's of meters depending on the system used. In summary, DAS measures strain-rate changes along fiber-optic cables that can be as long as 10's of km at spatial samplings of < 1 m, turning fiber-optic cables into massive vibration-sensing arrays.

Figure 3-1. Distributed Acoustic Sensing (DAS) measurement principle
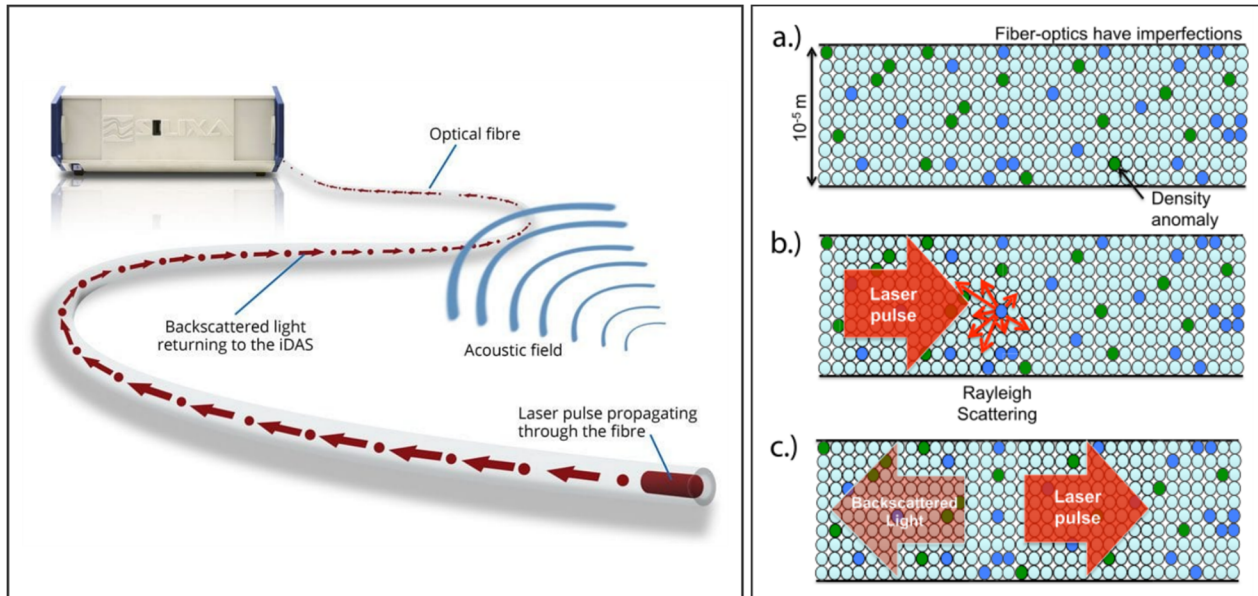
(Left) A DAS instrument connected to a fiber-optic cable measures vibrations impacting the cable by shooting laser pulses down the cable and recording the backscattered light that returns within the fiber to the instrument. (Right) Conceptual cartoon of the measurement principle of DAS; a) Impurities exist in the core of every fiber-optic cable, which cause small changes in refractive index; b) A laser pulse shot down the cable interacts with these impurities and Rayleigh backscattering occurs; c) The backscattered light returns to the instrument, as the laser light continues travelling down the fiber. Measurements of optical phase change on this backscattered light profile are transformed into changes in axial strain acting on fiber sections. Credit: left panel – Silixa; right panel: Lindsey et al. (2019).

Data Acquisition and Analysis

As previously mentioned, the main goal of the analysis presented here is to characterize the acoustic profile along the depth of the borehole at different times during the operation of the underground gas storage system using DAS. During a complete cycle of operations, the acoustic noise generated along the borehole will change its characteristics. During quiet times, noise level is expected to be low. On the contrary, higher amplitude noise will be recorded when gas is flowing through the well. Different injection pressures, flow rates, flow durations, etc. will generate different acoustic signals. By continuously recording and analyzing this noise, we can establish typical noise patterns for different stages of the operation, with the objective of determining what is "normal" and making it easy to detect an anomaly. Moreover, the high-spatial resolution of the measurements along the borehole will enable identifying localized anomalies.

The same fiber-optic cable used for acquisition of DTS data was used for the continuous recording of DAS data. A Silixa iDAS interrogator unit was installed in the same enclosure as the DTS system. Data have been continuously recorded between February 21st 2020 and the end of June 2020. Sampling frequency is 1 kHz (1e-3 s). Spatial sampling was 0.25 m up until March 19th, when it was increased to 1 m spacing with the goal of reducing data volume but still keeping the high-resolution needed for the analysis. Gauge length was 10 m and fixed in hardware. Data were

recorded in 30-seconds-long files and streamed continuously to 8 TB external hard drives and data was sent to LBNL by collaborators at SoCalGas. This acquisition has generated approximately 40 TB of data.

Figure 3-2 shows an example of a typical raw, 30-seconds-long DAS recording acquired during a time when no operations were taking place at the well. In order to map fiber channels into actual depth along the borehole, sequential hammer impacts were carried out at the head of the well. This test enabled matching a channel number with the head of the well (at position 0 m). The acoustic signals generated by these impacts can be observed as a distinct event at 8 s and as a series of sequential events between 20 s and 30 s in the record shown in Figure 3-2. Note that, in order to illustrate the geometry assignment procedure and the location at which the cable enters the well, the entirety of the cable is shown in Figure 3-2, including the portion of cable deployed on the surface running between the instrument and the wellhead. In the following sections, reference distance at 0 m will be the head of the well, in order to describe events in terms of true depth along the boreholes.

Figure 3-2. Example DAS noise recording
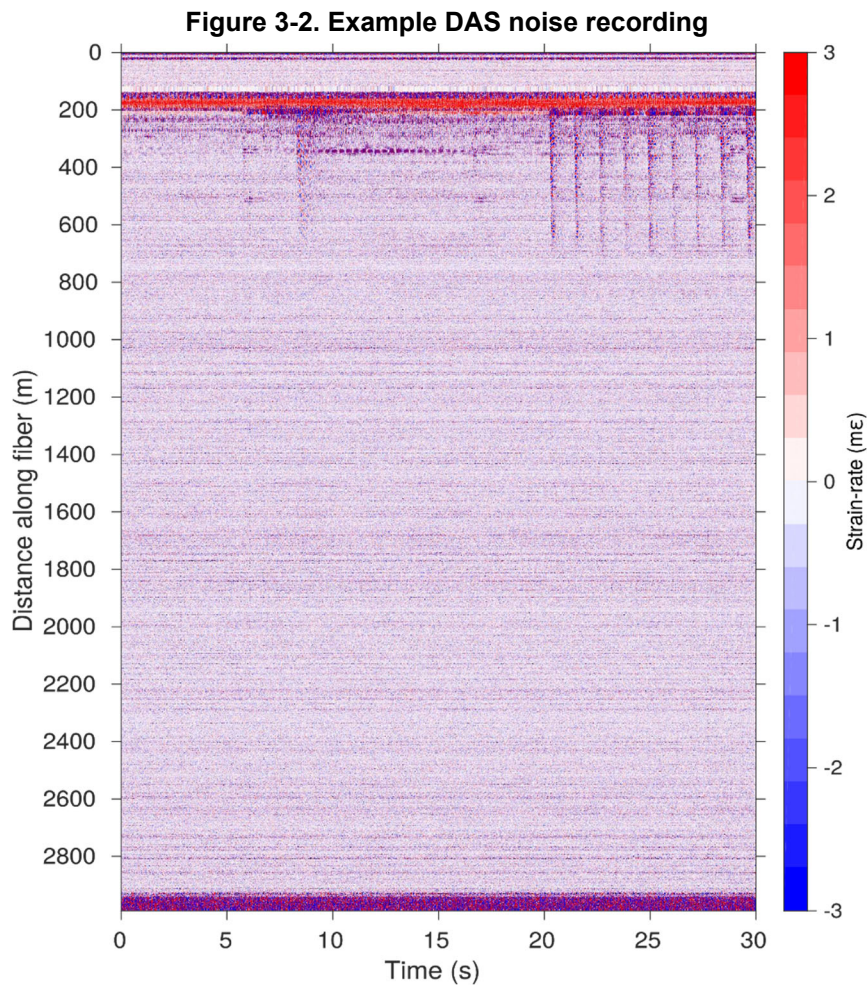
30-second-long raw DAS noise record along the length of the fiber optic cable. Change in noise pattern at approximately 80 m shows the location at which the fiber-optic cable enters the well. Discrete noise events propagating along the upper 500 m of the well correspond to hammer impacts at the well head, done to establish the geometry of the survey.

25

In the following sections, we describe our analysis of DAS data recorded before, during and after gas injection into the well for different injection tests occurring between February 21st and February 29th. For data analysis, we have followed two approaches. First, we investigate the first-order characteristics of the recorded raw noise. Data are converted from raw optical units to units of strain-rate, and amplitude and frequency characteristics of the acoustic noise are inspected. This analysis, described in Subsection 3.2.1 ('Raw Data Examination"), is informative and enables identification of first-order noise patterns. However, one can imagine how carrying this visual inspection for each individual 30-seconds-long file is time consuming and inefficient. Thus, our second approach consists of determining temporal and spatial variability of data attributes that can be easily calculated for each of these single recordings. These attributes can provide a more quantitative evaluation of noise characteristics, which can be used in the future to differentiate between "normal conditions" and "anomalous behavior." Details on the attributes selected, how they can be calculated and how they vary in space and time during operation cycles are described in Subsection 3.2.2. ("Determination of Data Attributes").

Raw Data Examination

One of the most straightforward approaches for characterizing noise patterns for the different stages in system operation is to analyze changes in amplitude (i.e., strain-rates) and frequency content of recorded noise. During quiet times, noise levels in the well are expected to be low, and its frequency content broad and constant. Changes in amplitude and frequency of the noise would indicate new sources of vibration, such as, for example, flow of gas or liquid during injection, withdrawal, or leakage incidents.

Here, we analyze and compare amplitude and frequency content of several 30-seconds long DAS noise records acquired at different stages of operation. Figure 3-3a shows tubing pressure at the analyzed well between February 22nd and February 29th, 2020. Based on this pressure record, we select an injection cycle starting on February 23rd and ending on February 24th, and analyze noise recorded during quiet periods (when no operations are occurring in the well), during gas injection into the well and during shut-in transient conditions. A close-up of pressure changes during this event and the exact times at which noise is evaluated are shown in Figure 3-3b. We should note that noise characteristics at these different stages of operations are common for all injection periods analyzed so far and the data shown here are representative of the acoustic behavior of the system throughout the time we have been monitoring noise using DAS.

As illustrated in Figure 3-4., the noise patterns recorded during quiet times, gas injection, and shut-in conditions are significantly different. During quiet conditions, noise levels are low and homogeneous along the depth of the borehole. This indicates that no significant sources of noise exist and mostly instrumental noise is present in the data. A very faint horizontal banding can be observed, which is most likely reflecting small differences in noise level at different channel locations, probably related to the coupling of the cable with the tubing. The 30-seconds-long noise record shown in the central panel of Figure 3-4, which was acquired about 45 minutes after injection starts, shows a much more complex noise pattern that changes not only in this short time but also along the depth of the well. The shallowest ~600 m of the cable are characterized

by very high amplitude signals with no clear interpretable waves. This signal is interpreted to be related to vibrations generated at the wellhead when gas is flowing and/or in transient conditions.

Figure 3-3. Tubing pressure record at the analyzed well during the period analyzed
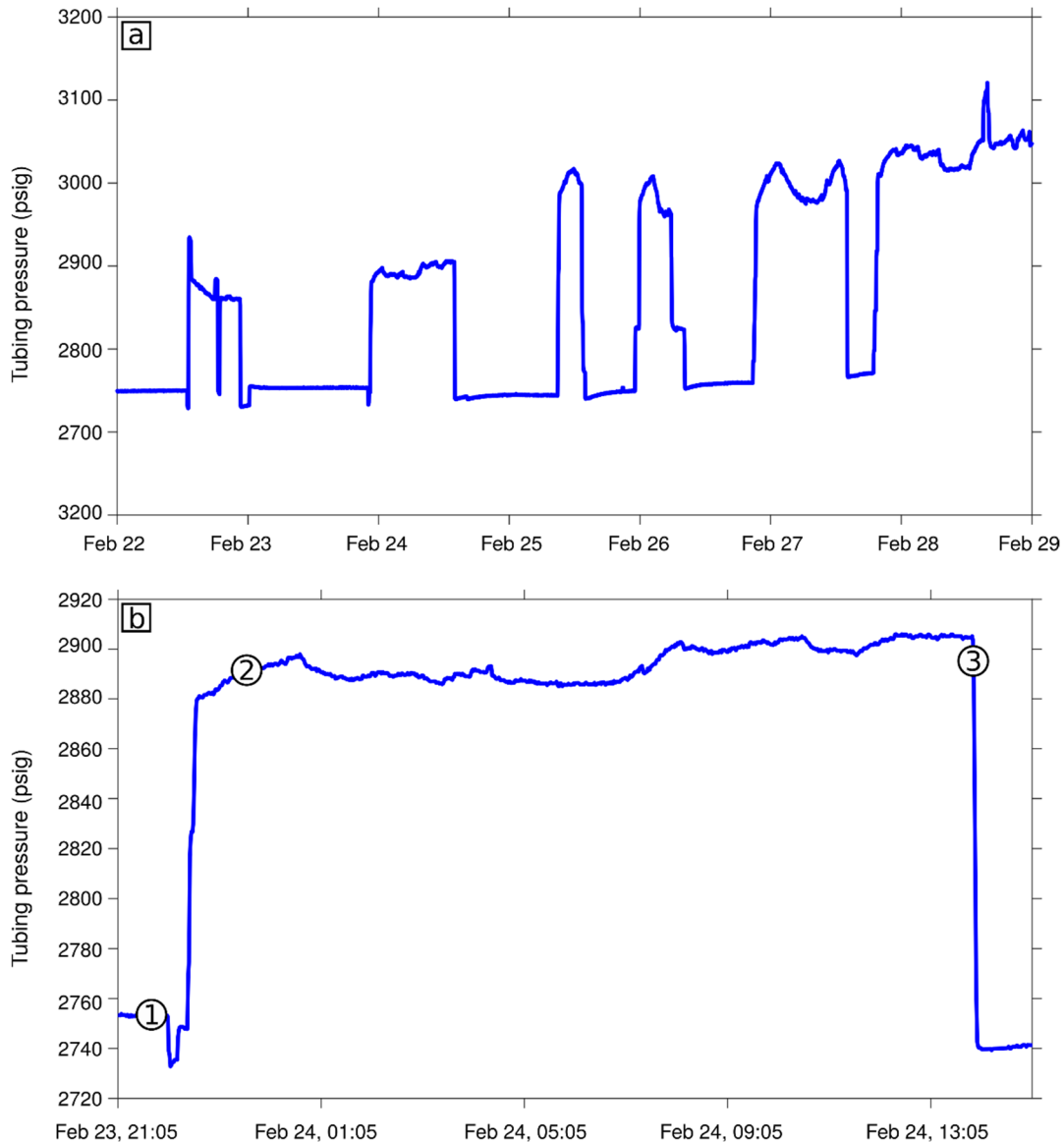
(a) Tubing pressure recorded between February 22nd and February 29th, 2020. (b) Close-up of tubing pressuring during injection of gas into the well between February 23rd and February 24th. Numbers in circles indicate recording times of DAS data files shown in Figure 3-4. 1 = quite period before injection; 2 = injection; 3 = shut-in transient.

The lack of clear seismic wave patterns is probably due to the intensity of the signal surpassing the dynamic range of the instrument. Additionally, this noise record is characterized by discrete acoustic events originating at a depth of ~1350 m and propagating up and down the well for

distances of ~400 m in both directions. These events are highly energetic and seem impulsive, with a duration of only 2 or 3 seconds. A closer examination of these events is described later in this section. During the shut-in transient, high amplitude noise can still be seen in the shallowest ~600 m of the well. A few discrete events are observed between depths of ~1000 m and ~1500 m. In contrast to the events observed during flowing conditions, however, these signals are less recurrent, less intense and they only propagate 50 m to a 100 m away from their origin point. These observations demonstrate that different stages of operations are characterized by different acoustic noise signals that vary in time and in depth along the well and that are easily recorded using DAS.

Figure 3-4. Raw DAS noise data acquired at three different stage of gas injection operation at time shown in Figure3-5b
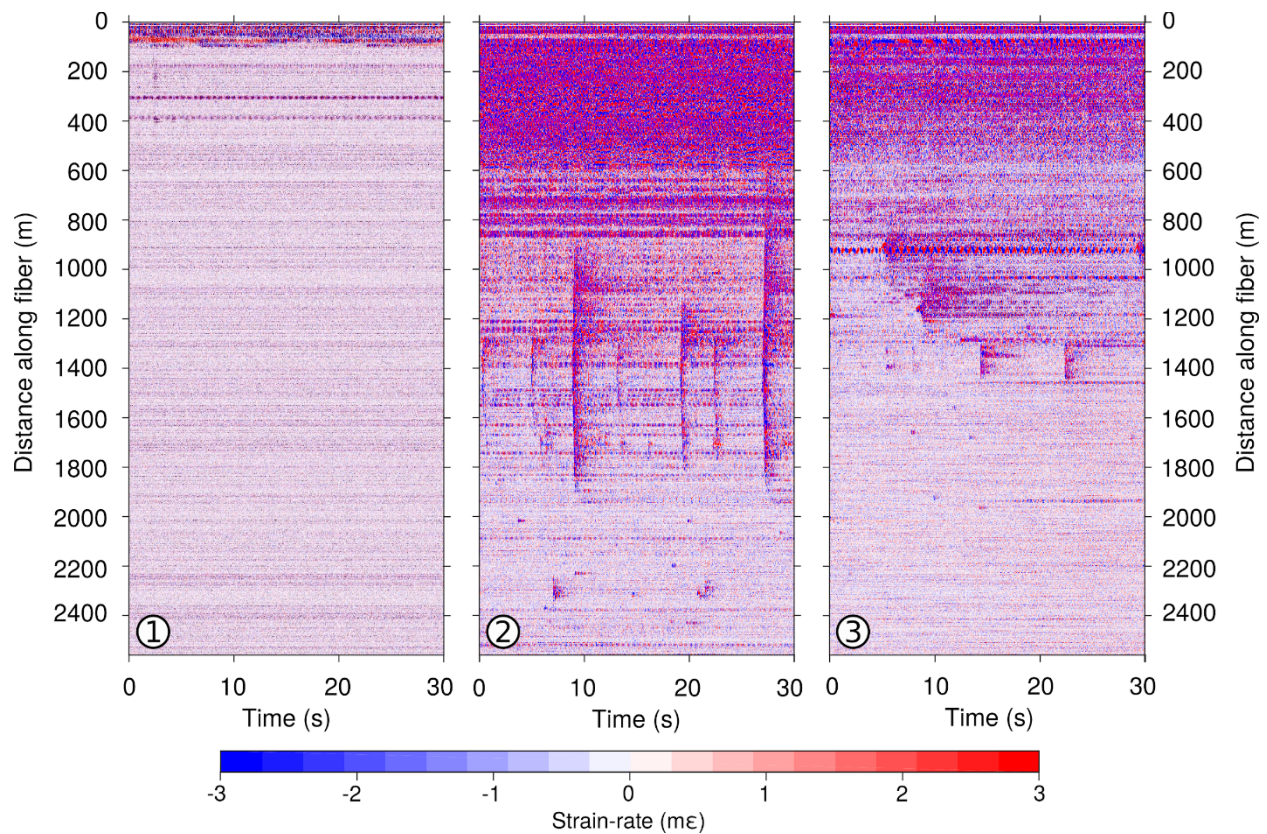
 (Left) 30-seconds-long DAS noise record along the well, acquired before gas injection starts. Note the absence of any significant acoustic signal. (Center) 30-seconds-long DAS noise record along the well, acquired 45 minutes after gas injection starts. Note high amplitude noise recorded in the shallower 600 m of the well, as well as discrete acoustic events occurring at depths between 1000 m and 1800 m. (Right) 30-seconds-long DAS noise record along the well, acquired during the shut-in transient. Amplitude of noise is lower, with fewer events.

As expected, variations in amplitude are accompanied by variations in frequency content. This is illustrated in Figure 3.5, which shows the spectral power of the noise records in Figure 3-4 for each measurement channel. When no operations are carried out, very low levels of ambient noise

28

are recorded, and hence the frequency spectrum of the recording is almost flat for all channels, i.e., there is no significant power at any particular frequency for any channel. During flowing conditions and during the shut-in transient, however, frequency content variations occur along the depth of the well. During injection, noise along the upper 600 m of the well is still broadband. High spectral power is observed at frequencies up to ~ 400 Hz. A similar pattern is observed at depths between ~800 m and ~2000 m, coinciding with the depths at which the discrete acoustic events are observed in Figure 3-4. At this depth, however, high amplitudes are only recorded up to 250 Hz. High spectral power peaks are observed at discrete frequencies, with an almost periodic character. This feature indicates that larger amplitude vibration occurs at these frequencies, suggesting some kind of resonant behavior in the system at those depths. During the shut-in transient, a similar behavior is recorded in the shallower 600 m of the borehole. At larger depths, peaks in spectral amplitude coincide with the depths of the discrete acoustic events observed in the raw amplitude data (Figure 3-4, rightmost panel).

Figure 3-5. Frequency spectra of DAS noise data shown in Figure 3-4
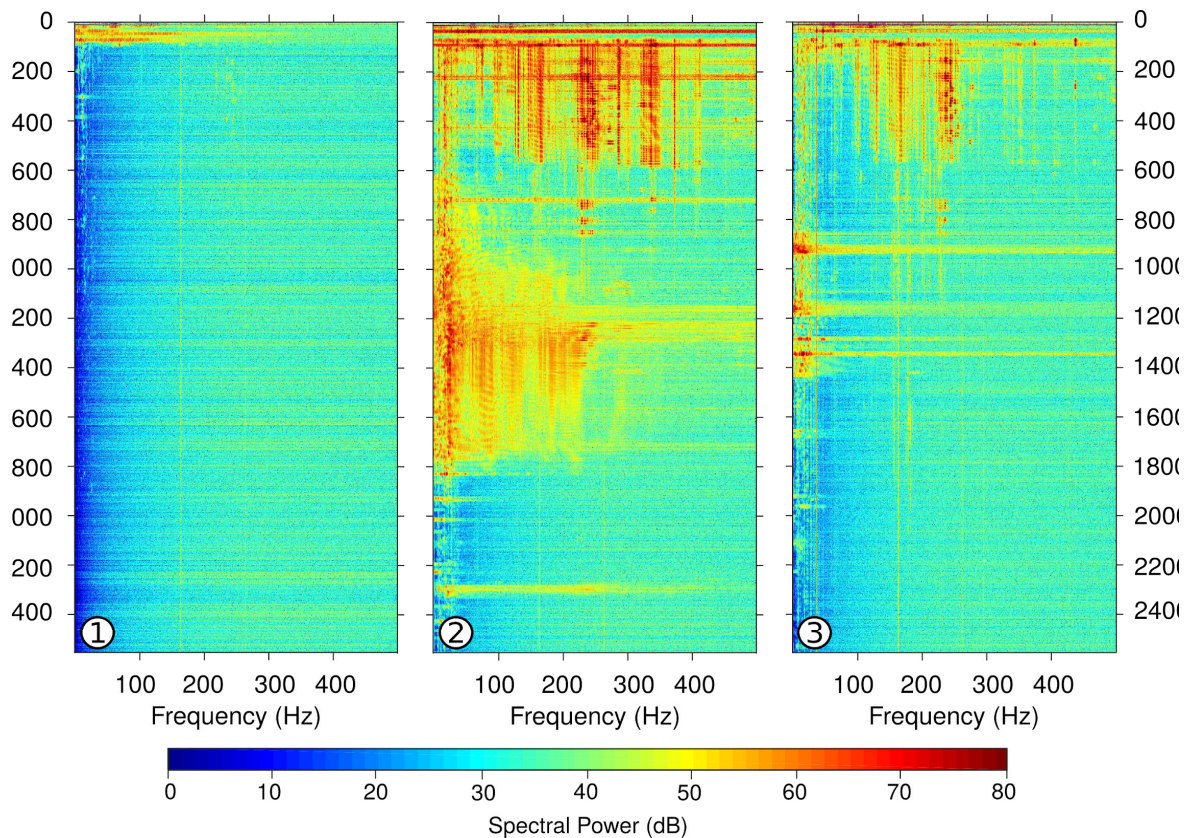
(Left) Spectral power of each channel along the fiber-optic cable for the 30-seconds-long DAS noise record shown in Figure 3-4 Left (acquired before gas injection starts). **(Center)** Spectral power of each channel along the fiber-optic cable for the 30-seconds-long DAS noise record shown in Figure 3-4 Center (acquired 45 minutes after gas injection starts). **(Right)** Spectral power of each channel along the fiber-optic cable for the 30-seconds-long DAS noise record shown in Figure 3-4 Right (acquired during the shut-in transient). For all three panels, note correspondence between high amplitude noise observed in raw noise records and an increase in spectral power at specific frequency ranges seen here.

29

In order to better characterize noise properties while gas is flowing, we analyze in more detail the discrete acoustic events observed during injection. First, we compare our DAS observations with the DTS measurements obtained along the same cable and described in the previous chapter of this report. Note that, because temporal resolution of DTS data is poorer than that of DAS (10 minutes for DTS as opposed to 0.001s for DAS), for this comparison we show DTS data acquired during the entire cycle of gas injection. Figures 3-6a and 3-6b show that the origin of most of these events is at a depth that is very close to the water-gas interface in the annulus as imaged by DTS. In panels c and d, a close-up of both datasets at depths between 800 m and 2000 m reveals that the acoustic signals originate ~200 m deeper than this interface; the DAS event originates at a depth of 1350, whereas the DTS data shows that the water-gas interface in the annulus is at 1200 m). Currently, it is unclear if a causal relationship exists between this interface and the acoustic events observed in the DAS datasets.

The close-up image of the acoustic events, shown in Figure 3-6c, reveals a very complex signal. The acoustic event originates at a depth of approximately 1350 m, but it propagates both upwards and downwards for distances as far as 600 m. This signal seems to have a very complex pattern of propagation, changing curvature and hence speed as it travels along the borehole. Notably, a polarity reversal is observed for this main arrival, as it is positive in the up-hole direction but negative in the down-hole direction. Secondary waves are recorded "emanating" from the main seismic arrival, propagating down the well only at very high speeds of 5000 m/s, which is the acoustic velocity of steel. This signal is probably revealing a complex interference of acoustic waves with the tubing walls, the flowing gas, and the fluid in the annulus. The origin of this acoustic signal is unknown at this point. An inspection of a variety of logs acquired along the borehole, such as caliper and cement logs, does not reveal significant features in the borehole at this depth. Further investigation is needed in order to fully comprehend the cause of these acoustic signals.

Figure 3-6. Close examination of DAS noise recorded while well is flowing and comparison with DTS data
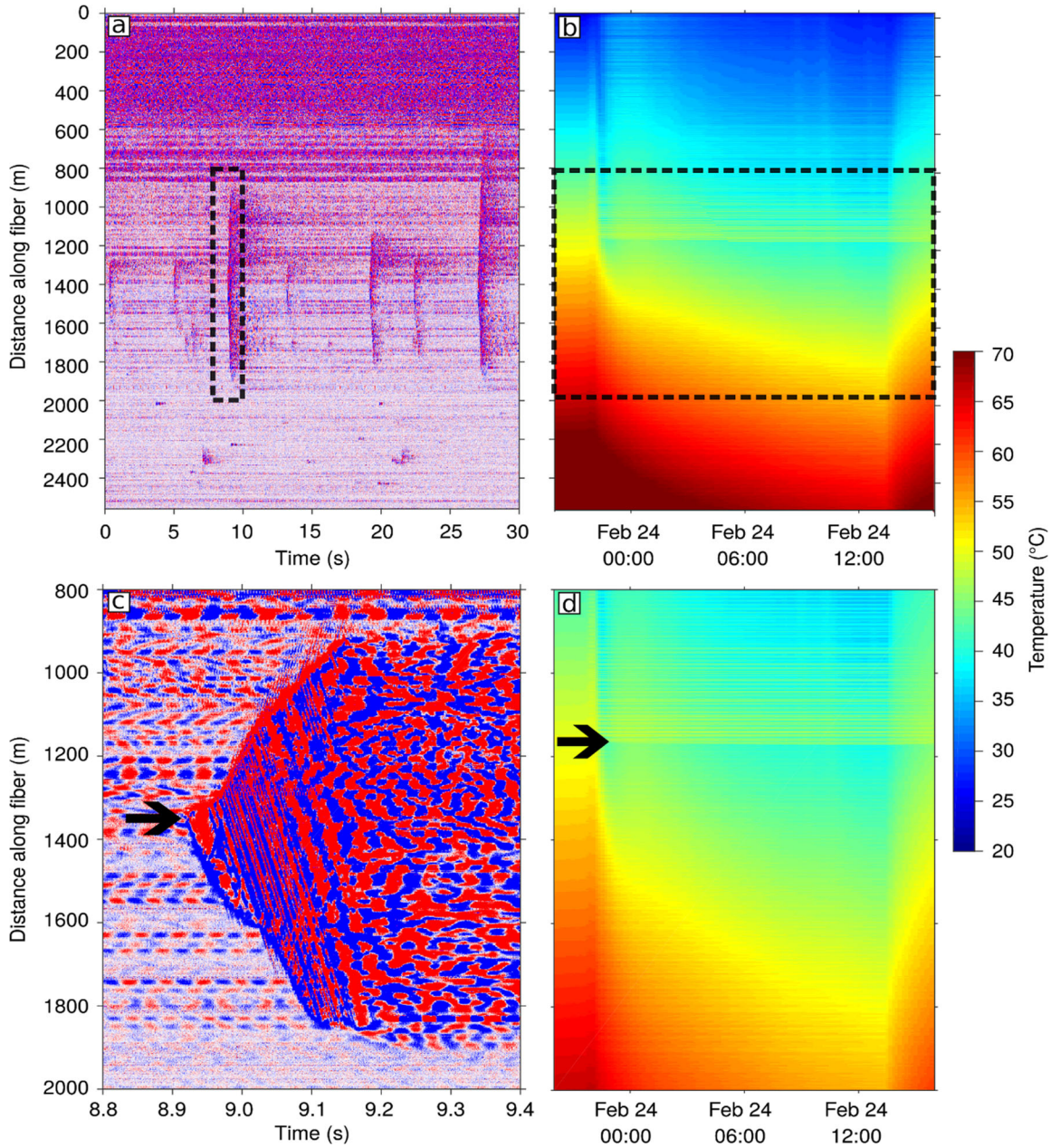
(a) 30-second-long DAS noise recorded acquired 45 minutes after well starts flowing. Dashed-line rectangle indicates region shown in panel c. (b) DTS temperature recorded during gas injection between February 23rd and February 24th (tubing pressure shown in Figure 3. 3b). Dashed-line rectangle indicates region shown in panel d. (c) Close-up of one of the acoustic events recorded during injection. Black arrow indicates depth location of the origin of the acoustic event at 1350 m. (d) Close-up of DTS temperature around the water-gas interface, for the same depth range shown for the DAS data in panel c. Black arrow points to depth of the interface.

Determination of Data Attributes

The observations reported in the previous section demonstrate that DAS is a powerful tool to continuously monitor the short-term and long-term behavior of UGS systems. Our analysis has shown that background noise generated in the well at different stages of operations can be recorded at high resolution using this technology, and it has revealed that changes in amplitude and frequency content are good indicators of changing conditions. Despite its utility, visual inspection of the amplitude and frequency content of each recorded 30-second-long file is very time consuming and inefficient. Moreover, the high density of measurements provided by DAS results in large data volumes that can be challenging to store and process. A simpler way of detecting changes in noise characteristics is by reducing each noise file to simple data metrics at each measurement channel that describe the main characteristics of the acoustic signal. Based on our previous analysis, we have chosen the following data attributes:

1. **Root-mean-square (RMS) amplitude per channel.** The square root of the sum of squared amplitudes at each time sample A_n divided by the number of time samples N:

$$RMS_{ch} = \sqrt{\frac{1}{N} \sum_{n=1}^{N} |A_n|^2}$$

   This attribute gives a measure of the energy at each recording channel, which will change through time depending on what is happening in the borehole.

2. **Centroid frequency per channel.** A weighted mean of the frequencies f contained in the signal. We calculate the centroid frequency by taking the Fourier transform of each channel and calculating a weighted mean of them, using the spectral power P at each frequency as the weight:

$$centroid_{ch} = \frac{\sum_{n=0}^{N-1} f(n)P(n)}{\sum_{n=0}^{N-1} P(n)}$$

This attribute provides an estimate of the "center of mass" of the frequency spectrum, which informs on the characteristics of the source of acoustic noise.

These attributes can be calculated in a few minutes for each 30-seconds-long file, and it significantly reduces the size of the data. However, they still contain critical information that describes the acoustic signal and enable fast identification of changing conditions in the system.

In this way, we obtain quantitative information on data amplitude and frequency content with a spatial density of 25 cm and a temporal resolution of 30 seconds for the entire recording period.

In Figure 3-7, we show RMS amplitude and centroid frequency of noise continuously recorded between February 22nd and February 29th, 2020. The topmost panel of Figure 3-7 shows tubing pressure throughout this period. The comparison of this record of gas injection with changes in RMS amplitudes and centroid frequency shows immediate correspondence of these noise attributes with perturbations in tubing pressure. For each injection, an increase in RMS amplitude is clearly observed immediately after the start of injection. Along the shallower section of the borehole down to ~ 600 m, high amplitude noise is recorded for the entire injection period. This region becomes very quiet (i.e., noise amplitude is very low) as soon as the well is shut in. A similar behavior is observed at some depths in the range of 600 m to about 950 m. In this region, RMS amplitudes are slightly lower and not as continuous in depth. However, they are also recorded for the entire time while the well is flowing. Deeper in the well, at depths characterized by those discrete acoustic events observed in the raw noise data shown in Figure 3-4, high amplitude noise appears to occur as soon as injection starts, but it is mostly restricted to the first 1-2 hours in which the well is flowing. This behavior suggests that acoustic signals are generated when tubing pressure is increasing (i.e. when gas starts flowing) but acoustic emissions decrease substantially once pressure is stabilized. A small increase in the RMS amplitude at these depths is briefly observed during the shut in transient, but it is not as obvious as for the start of injection.

Variations in the centroid frequency follow the same pattern as the changes in RMS amplitude, as expected. This high-amplitude noise is characterized by a shift to lower centroid frequencies, which indicate that these acoustic signals have lower frequency than the noise recorded during quiet times, which is mostly instrumental. Interestingly, centroid frequency values go back to higher frequencies almost immediately after the first injection in February 23-24. After all other injections, however, centroid frequencies do not recover as much and stay at slightly lower values than "normal", which might suggest a long-term perturbation of the acoustic field. Additionally, centroid frequency variations are observed while the well is flowing at large depths in the range of 2000 m to 2400 m (bright blue spots at those depths), with almost imperceptible changes in RMS amplitudes.

Figure 3-7. Data attributes for the recording period between February 22nd and February 29th
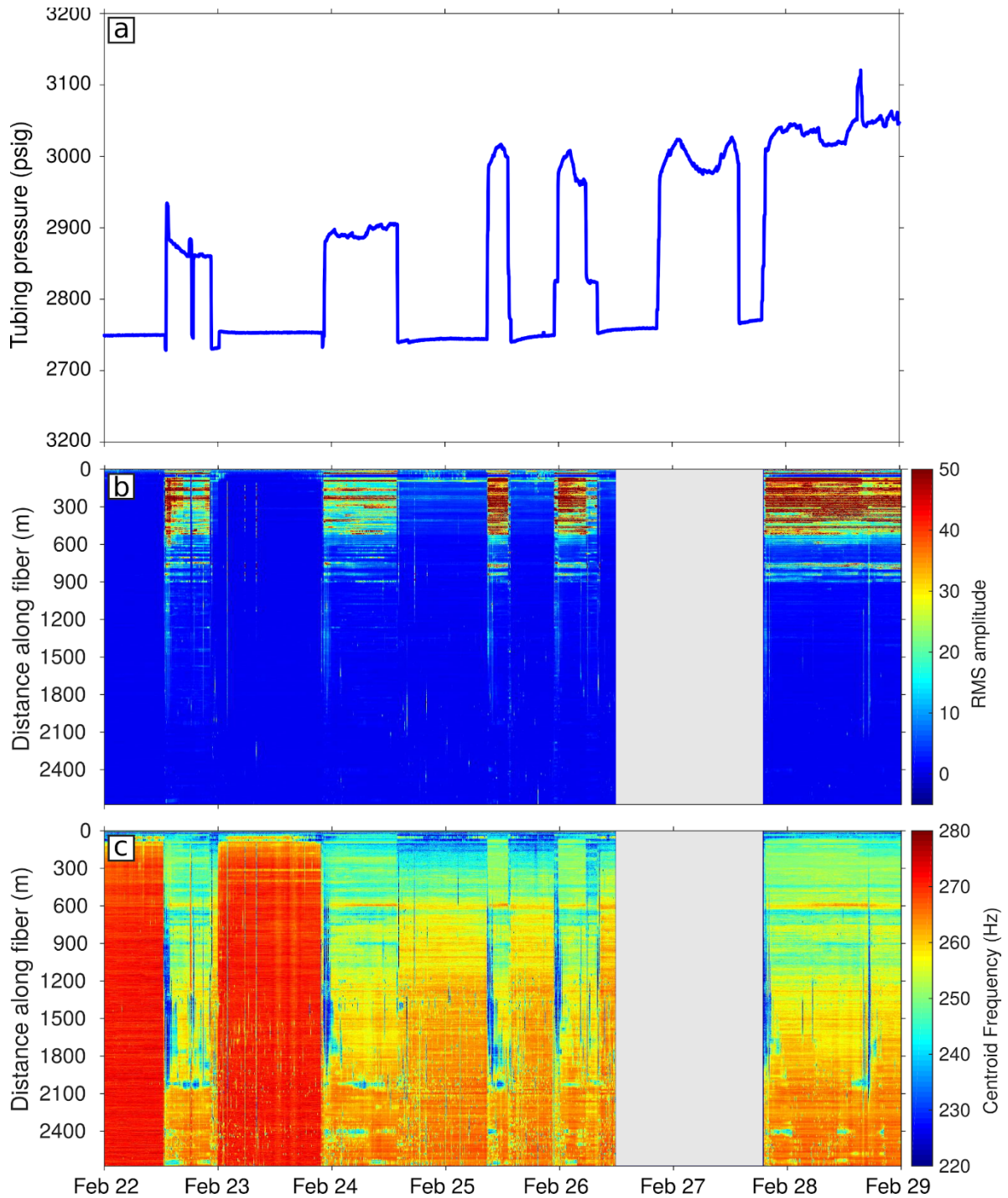
(a) Tubing pressure for period between February 22nd and February 29th. (b) Rot-Mean-Square (RMS) amplitude for all data recorded during this period. Note how high amplitude periods correspond to times at which the well is flowing. Gray band indicates period with no data (c) Same as panel b, but showing centroid frequency. As in b), gray band indicates a gap in the data record. Note a shift in centroid frequency to lower frequencies during flowing conditions.

Summary and Conclusions

This preliminary analysis of acoustic noise data acquired using Distributed Acoustic Sensing (DAS) demonstrates that this technique can be a powerful tool to monitor the performance of underground gas storage (UGS) systems. DAS technology converts fiber-optic cables into massive arrays of seismic sensors that record the acoustic field at very high spatial and temporal resolution with minimal effort. Data can be recorded along the borehole at spatial density as high as 25 cm. Measurements can be made continuously in an unsupervised manner, as long as the instrument can be connected to a source of power and there is an adequate data storage system in place. These features make DAS a promising tool for long-term monitoring of UGS. It may take some time for utilities to deploy the technology. In addition to the high cost, DAS monitoring is still in the research stage and data interpretation needs expertise.

Our observations indicate that the analysis of acoustic noise recorded by DAS can provide critical information about changes occurring in the borehole at different stages of system operation. In our analysis, we have been able to characterize these different stages, with the objective of setting background characteristics that describe the acoustic behavior of the system during normal operations. This knowledge will enable establishing what "normal behavior" is, so that anomalies are quickly identified and analyzed to search for malfunctions such as a leak. As stated in our introduction to this chapter, leaks are expected to generate characteristic acoustic signals that could be disentangled from the "normal" noise field.

With our data exploration approach, we have identified data attributes that can be quickly calculated for each DAS data file and can provide insights into spatial and temporal changes in the borehole. Such capability could be deployed in IRMDSS. By continuously calculating the RMS amplitude and centroid frequency at each measurement point with a resolution of 30 s, we could identify anomalous behavior, release a warning and contrast the DAS observations with additional data streams (such as DTS, InSAR, etc.) to evaluate the potential for a hazard. Ongoing work in this framework regarding DAS will entail gaining a better understanding of the origin of the acoustic events observed while the well is flowing, and integrating the DAS capability into the IRMDSS system.

CHAPTER 4:
InSAR Monitoring

Introduction

Long term monitoring of the performance of an underground gas storage (UGS) system is only possible if a cost-effective technique is available to detect changes that are indicative of issues such as well leaks, fault motion, and landslides. Interferometric Synthetic Aperture Radar (InSAR) is one such approach, as the data are often freely available or available at low cost for uses such as hazard mitigation. The satellites can be used to detect ground motion at the surface of the Earth at near weekly or monthly sampling rates. The ground deformation may be due to many causes, such as groundwater pumping and excavation, but well leaks and reservoir leaks and fault motion can also produce detectible surface movements. In this section we describe our development of a workflow for detecting anomalous ground deformation that suggest unusual behavior that warrants further examination. We have developed this approach and applied it to both field observations and synthetic test data.

The monitoring of the underground storage of natural gas is a more recent development (Teatini et al. 2011) and is still relatively rare. That is, of the over 600 underground gas storage sites in the world only a handful have documented monitoring programs. All of the studies document observable surface deformation, of the order of a few millimeters to a few centimeters, that is correlated with the seasonal activity of the storage facility. One unpublished study by MDA for Southern California Gas Companay (MDA 2013) was conducted for a gas storage facility at Playa del Rey in California. Though the study did record some deformation over the storage area, the deformation is attributed to soil moisture changes and not to the operation of the facility.

Description of Interferometric Synthetic Aperture Radar (InSAR)

Interferometric Synthetic aperture radar (InSAR) methods rely on the phase delay of a reflected microwave or radar wave to estimate the change in distance over time from the satellite to distinct points on the Earth's surface (Figure 4-1).

Figure 4-1. Schematic showing the principle underlying the estimate of range change from Synthetic Aperture Radar observations from an orbiting satellite
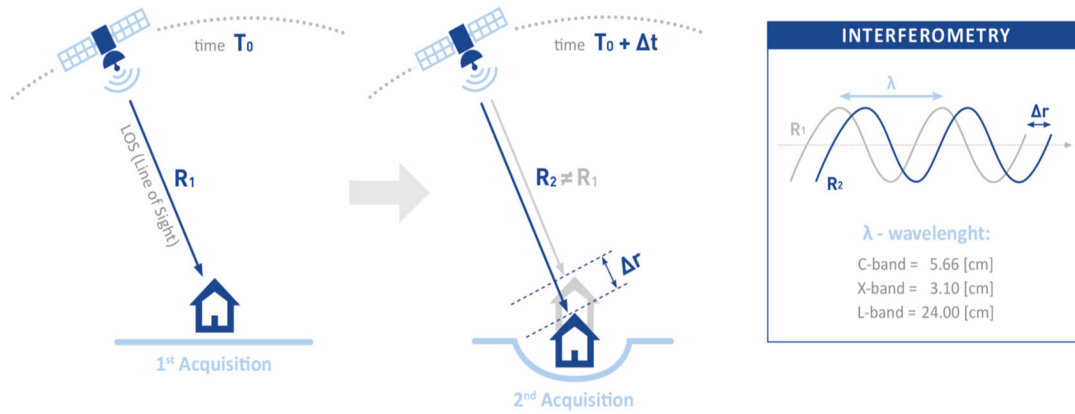
Both airborne and satellite-based systems are available and the methodology is now well established and widely used to map the deformation of the Earth's surface (Ferretti 2014). The accuracy of InSAR measurements depends on a variety of factors including spatial (i.e., distance between subsequent satellite passes) and temporal (i.e., time span between two acquisitions) baselines, satellite wave-length, land cover, and atmospheric conditions. To better understand the nature of InSAR observations, consider the phase of a pulse reflected from a point on the Earth, a single pixel in a SAR image (Figure 4-1). The phase value φ of a pixel P of a radar image can be modeled as a mixture of four distinct contributions (Ferretti 2014):

$$\varphi(P) = \vartheta + \frac{4\pi}{\lambda}r + a + n \qquad (4\text{-}1)$$

where ϑ is the phase shift related to the location and to the reflectivity of all elementary scatterers within the resolution cell associated with pixel P. The coefficient $4\pi r/\lambda$ is the most significant contribution in any geodetic application, as it is associated with the sensor-to-target distance or range, r. The term a is a propagation delay introduced by variations in the Earth's atmosphere. This quantity is often the main source of error and can compromise the quality of any distance estimate. The last term, n, is a phase contribution related to system noise such as thermal vibrations, quantization errors, and so on. The phase values contained in a single SAR image are of little practical use, as it is impossible to separate the different contributions in Equation 4-1 without prior information. The basic idea of SAR interferometry is to measure the phase *change*, or interference, over time, between two radar images, generating an *interferogram I*:

$$I = \Delta\,\varphi(P) = \Delta\,\vartheta + \frac{4\pi}{\lambda}\Delta r + \Delta a + \Delta n \qquad (4\text{-}2)$$

If we consider an idealized situation where the noise is negligible, the surface character and atmospheric conditions are constant between the two SAR acquisitions, then Equation 4-2 reduces to

$$I = \Delta\,\varphi(P) = \frac{4\pi}{\lambda}\Delta r \qquad (4\text{-}3)$$

Therefore, if a point on the ground moves during the time interval between the acquisition of the two radar images with similar geometry, the distance between the sensor and the target changes, creating a phase shift proportional to the displacement (Figure 4-1).

The literature on InSAR techniques and applications is vast and several techniques have been developed to improve the calculation of range change. Two of the more promising approaches that have led to estimates with a precision of several milli-meters are permanent or persistent scatterer techniques and small baseline analysis. Both methods use a sequence of inteferograms to overcome the limitations of conventional InSAR analyses, namely: phase decorrelation, i.e., possible changes in the radar signature over the area of interest, the term ϑ in Equation 4-2, and atmospheric effects. The first method relies on the identification of point-wise, coherent, radar targets, often referred to as permanent or persistent scatterers (Ferretti et al. 2001). Permanent scatterers correspond to radar targets with relatively constant amplitudes and slowly-varying phase that can be either natural or man-made. The Small Baseline Subset (SBAS) method (Berardino et al., 2002, Lanari et al. 2004, Hooper 2008, Samsonov et al., 2011, Samsonov and d'Oreye 2012) selects many coherent interferograms acquired with small spatial and temporal baselines, solves for the deformation rates between subsequent SAR acquisitions, and then reconstructs time series of the cumulative displacements.

Analysis of RadarSat-2 InSAR Observations at the Honor Rancho Gas Storage Site

There are several sets of InSAR satellite systems available for use in the monitoring of ground deformation above gas storage sites such as at Honor Rancho (Figure 4-2).

These systems have different characteristics, such as re-visit times, cost, radar central frequency, and the look direction. For example, Sentinel-1 data from the European space agency is available at no-cost for non-commercial uses. For our analysis at Honor Rancho we utilized observations from the RadarSat-2 system operated by the Canadian government. These data were acquired, and the data reduction, were done at no-cost by our collaborators in this project. Some characteristics of the RadarSat-2 system are noted in Figure 4-3. The repeat time of 24 days allows for nearly monthly observations. The accuracy of the estimates of surface displacement, in this case in the direction of the satellite position as it samples the area, is of the order of a few milli-meters relative to a nearby stable base point.

Figure 4-2. InSAR satellite systems available since mid-2006

Available InSAR data sets

	2006	2007	2008	2009	2010	2011	2012	2013	2014	2015	2016	2017	2018	2019

ENVISAT

CSK-A   (night acquisition)
CSK-D

TSX-A
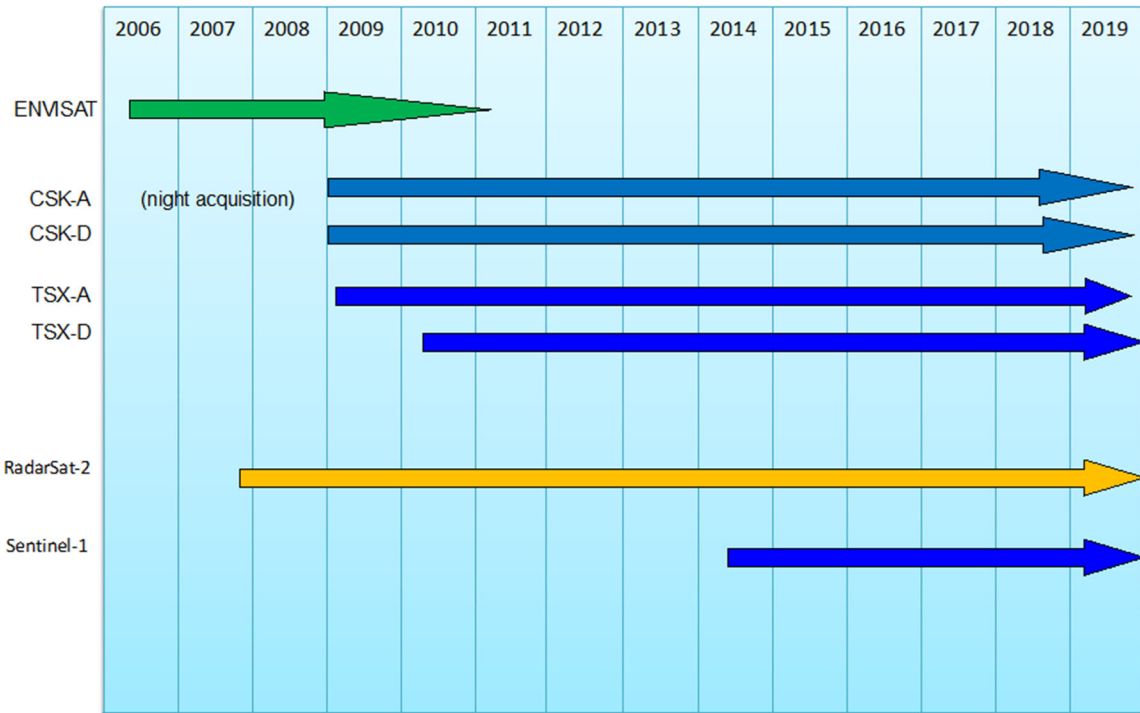TSX-D

RadarSat-2

Sentinel-1

Figure 4-3. Map showing the frame from the track that covers the Honor Rancho gas storage facility

RadarSat-2
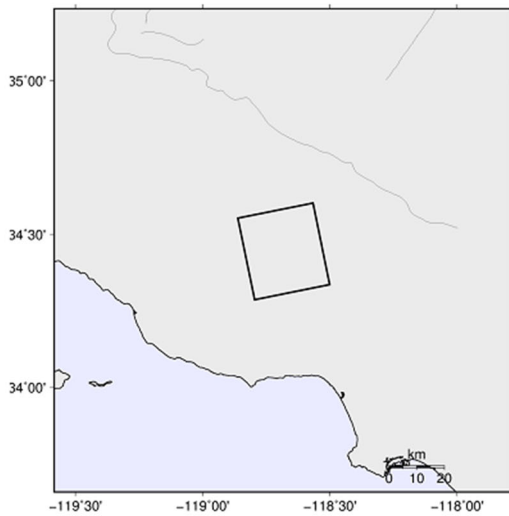
- Operated by the Canadian Space Agency

- One satellite track covers the Honor Rancho

- Repeat time of 24 days

- Observations are not free in general

Figure 4-4. Temporal and spatial baselines for InSAR data

RadarSat-2
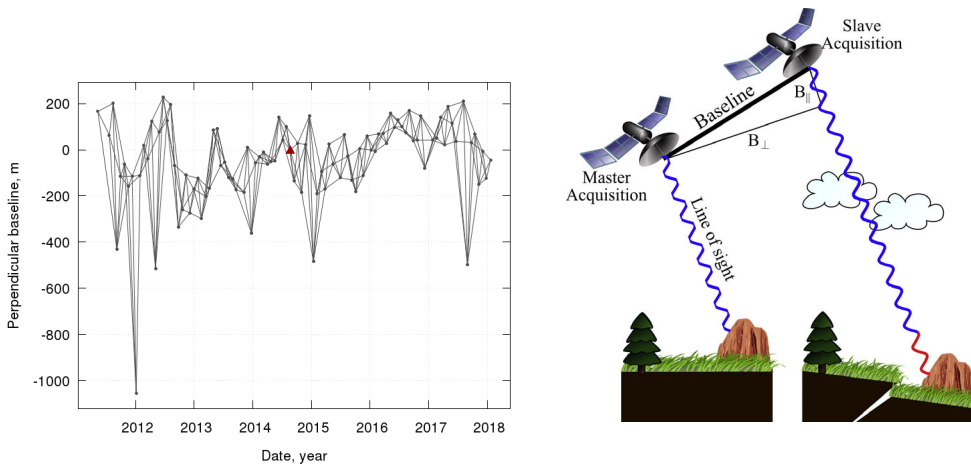
Figure 4-5. Satellite image of area around Honor Rancho and range changes
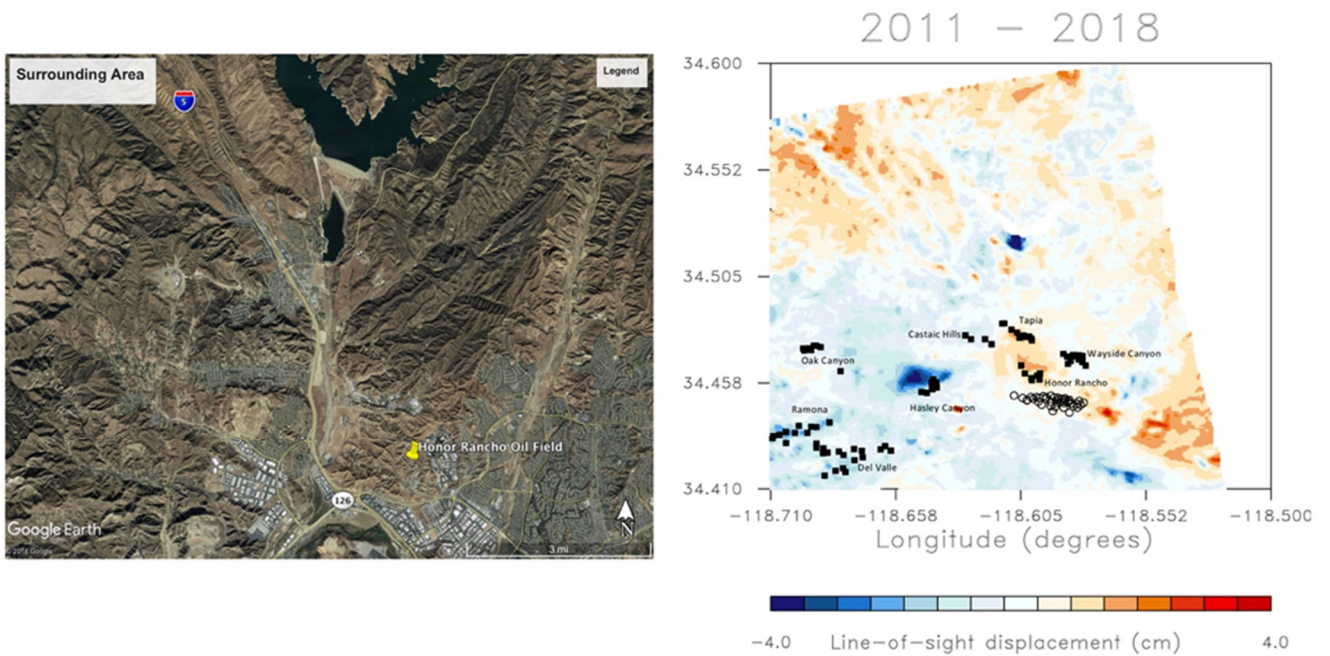
Left-hand-side: satellite image is from google maps. Right-hand-side: range changes in the region around Honor Rancho. Active oil wells are indicated by the filled squares and Honor Rancho gas wells are denoted by the open circles.

InSAR data from early 2011 until the start of 2018 were used in the field testing of the approach for detecting anomalous events. The processed data were obtained from our collaborator at Natural Resources Canada, Sergey Samsonov. The Small Baseline Subset (SBAS) technique was used to obtain estimates of range change, a change in the distance to the satellite for all of the 24-day time intervals for this period. As noted above, in the small baseline approach pairs of images that are close in space and time are used to estimate corrections for things such as topography and atmospheric effects. The baselines over time are

40

shown in Figure 4-4. Application of the SBAS method produced estimates of range change for a large area encompassing the Honor Rancho gas storage facility. Line-of-sight (LOS) displacements (range change) indicate movements exceeding 4 cm over the entire seven-year period (Figure 4-5). Negative values of LOS displacement correspond to subsidence.

The area displays a complicated pattern of range changes with some evidence of tectonic activity and indications of subsidence associated with the oil fields. If we focus more closely on the Honor Rancho area (Figure 4-6), we notice general uplift over the area around the UGS field.

Figure 4-6. Close up view of the range change estimates in the region of the Honor Rancho gas storage facility (negative LOS is subsidence)
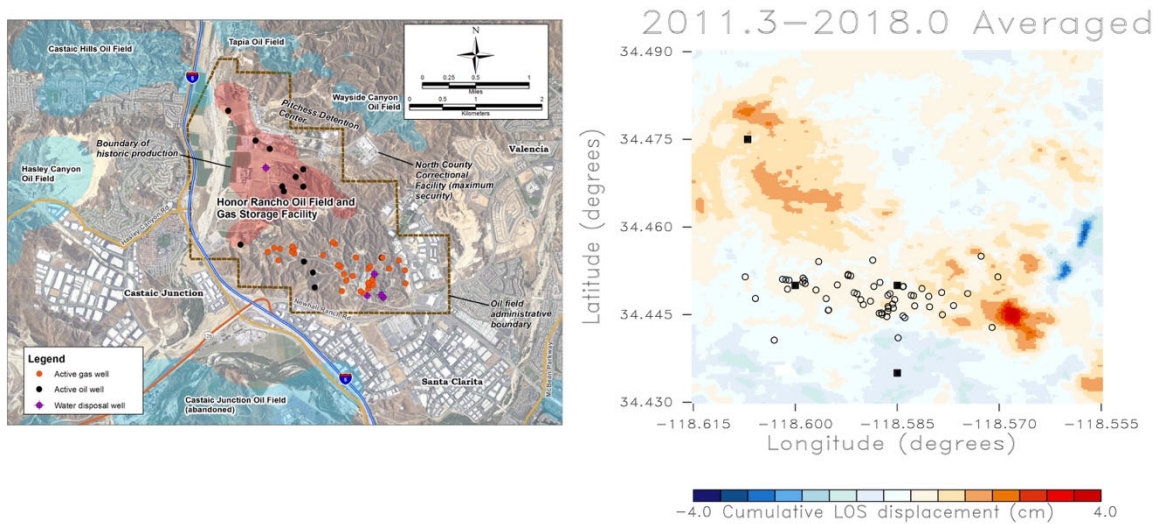
Left-hand-side image is from: https://en.wikipedia.org/wiki/Honor_Rancho_Oil_Field#/media/File:HonorRanchoDetail.jpg

A Comparison with Sentinel-1 InSAR Observations

We also worked with U. C. Berkeley to analyze Sentinel-1 SAR data using a persistent or permanent scatterer approach. As noted above, and indicated in Figure 4-7, in this method stable scatterers are identified and range changes associated with those objects are estimated. Thus, poorly constrained or characterized objects are thrown out and we focus on objects whose amplitude and phase vary slowly in time.

The technique was applied to data from the European Space Agency's Sentinel-1 satellite. The resulting range changes for the four-year interval 2015 to 2019 are shown in Figure 4-8 where they are compared with the earlier SBAS estimates. The estimates are roughly comparable; disagreement is to be expected given the significantly different time intervals of the data. The persistent scatterers are much more widely dispersed and appear to be more variable than are the SBAS estimates.

Figure 4-7. Intuitive idea underlying the persistent scatterer approach

Processing scheme: **P**ersistent **S**catter (PS) analysis

Distributed scatterer pixel   "Persistent scatterer" (PS) pixel
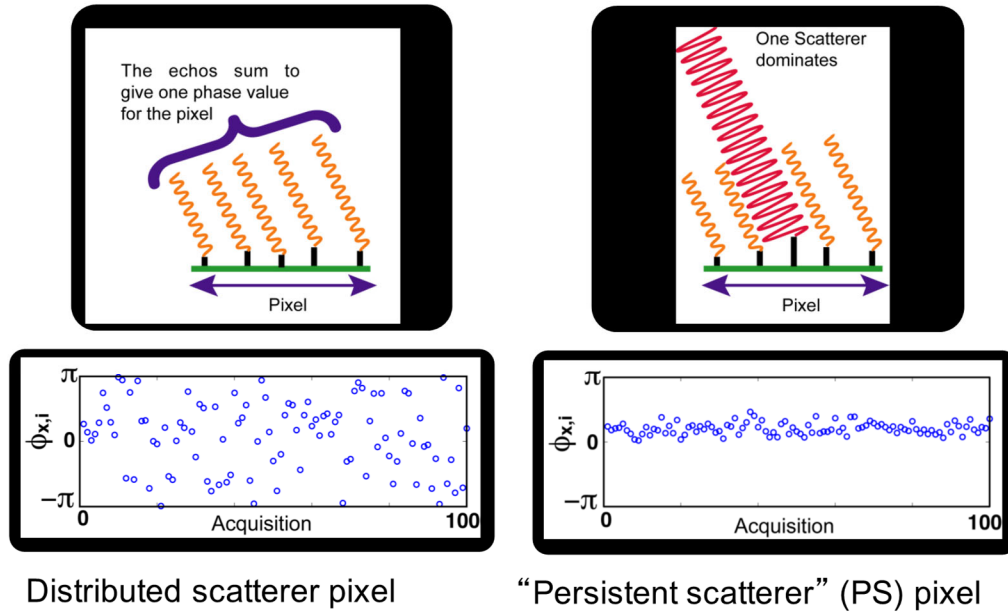
Figure 4-8. SBAS estimates from RadarSat-2 data (left) and estimates of range change for persistent scatterers identified from Sentinel-1 data (right)
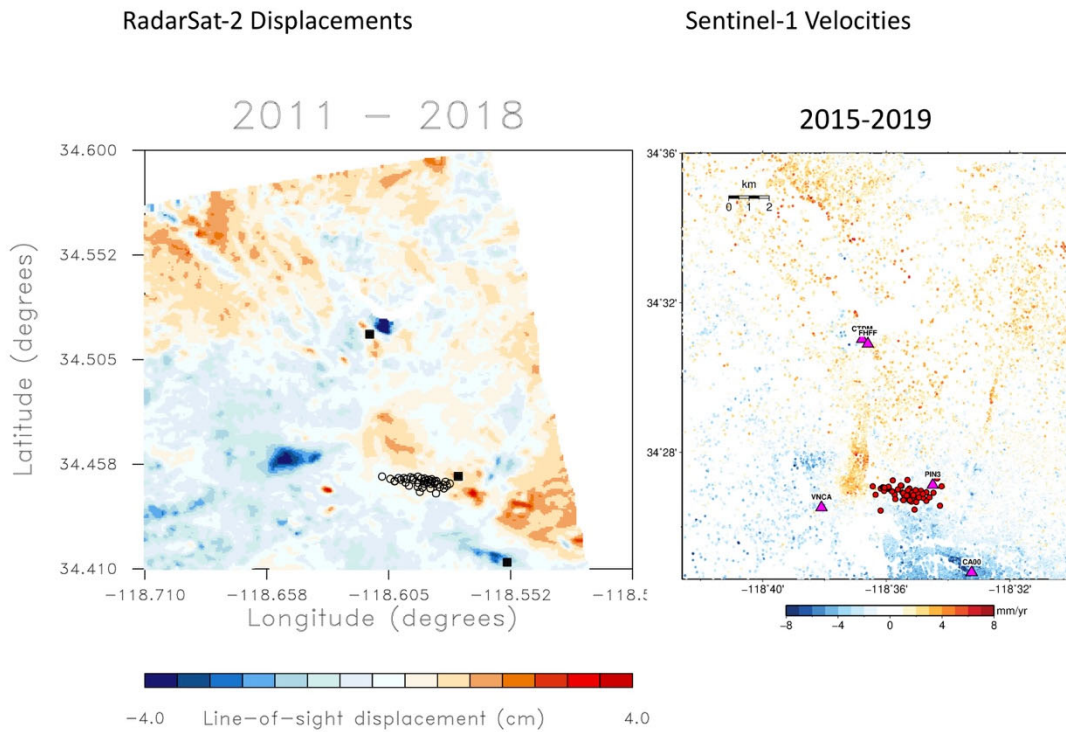
A Comparison with Data from the Global Positioning System

In order to validate the RadarSat-2 range change estimates we compared them to observations from nearby Global Positioning System (GPS) instruments. The Global Positioning System is a constellation of satellites, originally deployed by the U. S. military, for accurate positioning of points on the Earth's surface using sophisticated triangulation (Figure 4-9). There were three stations in the general vicinity of the Honor Rancho gas storage site (Figure 4-10). From this figure one observes the significant variation in the range change with location in the region. The GPS instruments give all three components of displacement of points on the Earth's surface. Using the look direction, we can project the displacement vector onto the look vector to obtain estimates of range change for each instrument as a function of time. In Figure 10 we compare the range change estimates for each instrument. There is general agreement between the two data sets.

Overall there is considerable scatter in the range change estimates though the systematic change at CA00 are systematically larger than the scatter.

Figure 4-9. Cartoon illustrating the general characteristics of the GPS

6 visible satellites
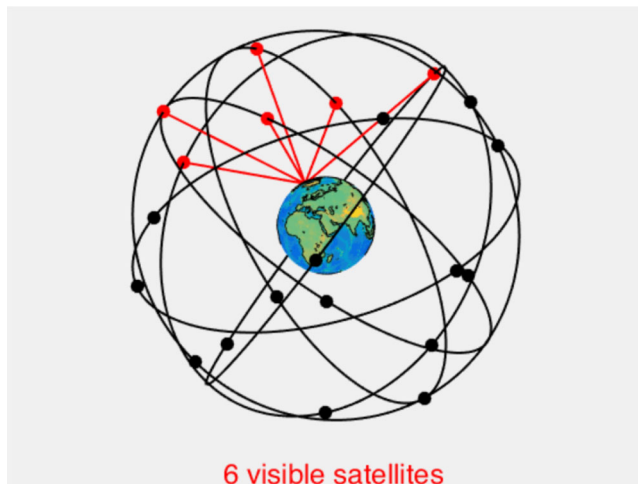
Figure 4-10. Comparison of InSAR range change and GPS estimates of range change

SKYB

PIN3

CA00
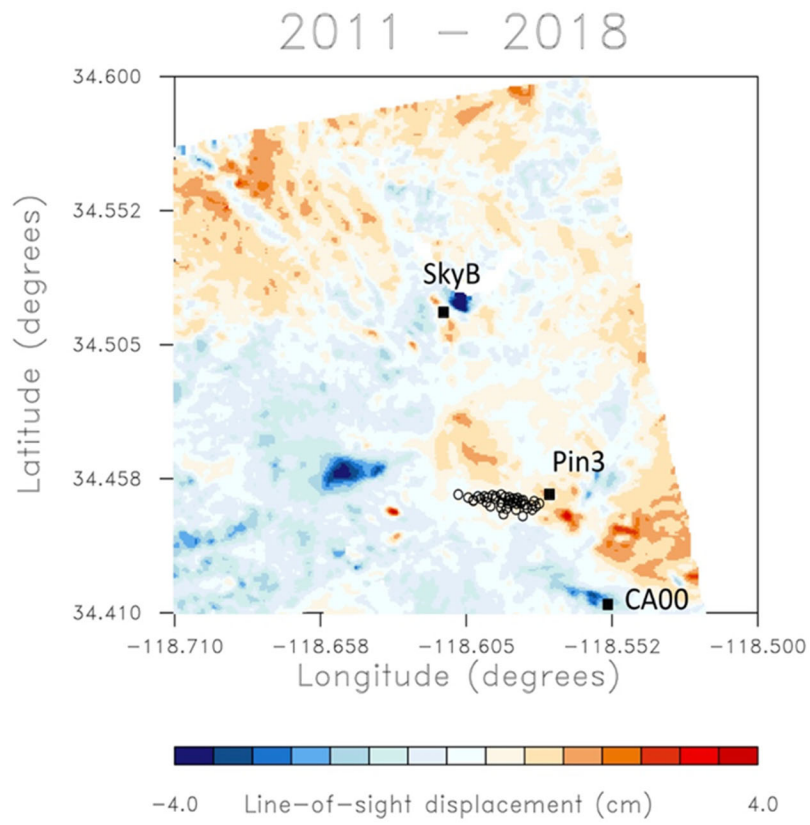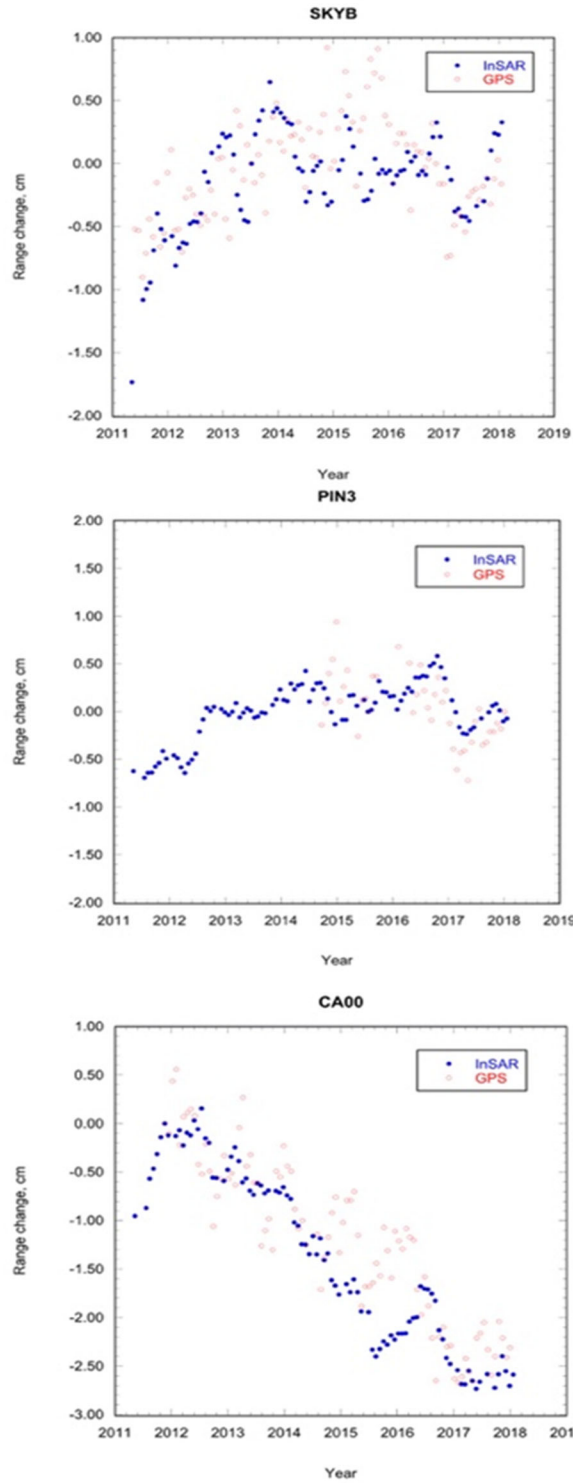
Upper figure shows the location of the three GPS instruments with respect to the Honor Rancho gas storage site. The lower three figures show range changes estimated using GPS displacement observations compared with InSAR estimates.

A Workflow for Identifying Anomalous Events

The monitoring system needs to flag unusual behavior in a relatively automatic fashion and, once it is up and running, should not require expert intervention on a routine basis. With this in mind we developed an approach to classify observed displacements as routine and anomalous. The basic idea is to set up a mechanical model of the reservoir-overburden system. Using the reservoir boundaries determined by the well intersections (Figure 4-11) we can define the reservoir top and bottom. Similarly, we can define the intersections with the major layers of the overburden.

Figure 4-11. Top boundary of the gas storage interval at Honor Rancho
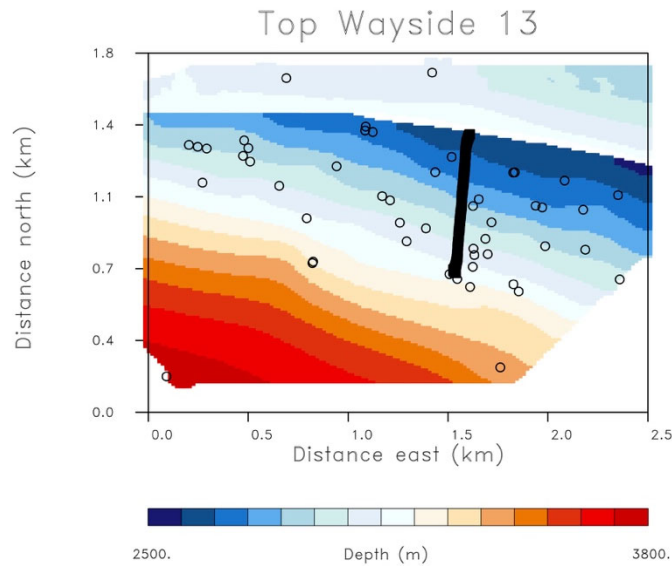
The well intersections with the boundary are plotted as open circles. The line of filled squares signifies the trace of the well containing the compressional and shear sonic logs used to construct an elastic model of the overburden.

In this manner we can construct a fully three-dimensional elastic model describing the reservoir, the overburden, and the underburden. A vertical slice through the top 4 kilometers of this model is plotted in Figure 4-12.

Figure 4-12. Cross-section through the top portion of the elastic model
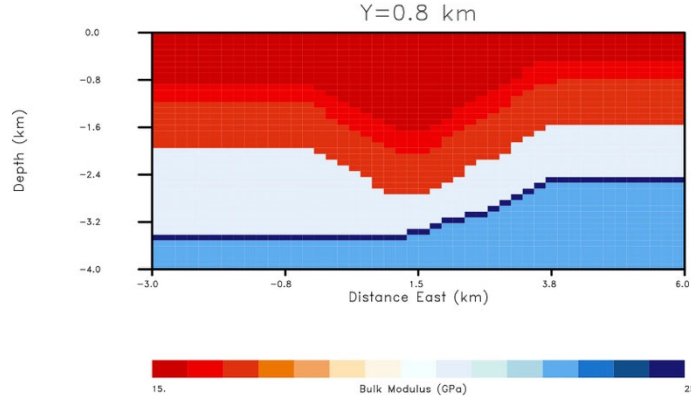
Cross-section through the top portion of the elastic model derived using the boundaries derived from well intersections and the elastic properties from the log in the well shown in Figure 4-11. The reservoir interval corresponds to the thin dark blue layer near the base of the model.

Changes in the fluid volume, due to gas injection and withdrawal, within the reservoir lead to variations in the effective pressure, that is the difference between the total pressure and the fluid pressure, inducing deformation and stress changes within the reservoir and the surrounding rock. Under favorable conditions the resulting stress and strain lead to observable surface deformation. To make use of these observations we need to relate the surface deformation to reservoir processes. There are several levels of sophistication that can be used to describe this relationship. At the simplest level, we can relate the surface deformation directly to reservoir volume change without considering the fluid pressure changes that led to the volume change. Thus, we restrict ourselves to purely mechanical considerations and are not concerned with modeling the fluid flow leading to the volume change. This approach involves the fewest model parameters, and if we are interested in short time intervals, the approach can usually be carried out using an elastic or poroelastic model for the overburden (Vasco et al. 2010). More sophisticated simulations of the fluid flow within the reservoir can improve the fidelity of the modeling, at the expense of introducing additional, often unknown, parameters such as reservoir permeability and porosity. The most advanced level involves modeling both the fluid flow and the deformation using a coupled numerical simulator

The simplest conceptual model used to relate the deformation to volume changes in the reservoir is similar to that applied in seismic source estimation and imaging. That is, though the source volume may undergo non-linear deformation and strain, outside of the source region the much smaller deformation of the surrounding rock can be described using methods from linear elasticity over the time interval between surveys, typically less than one month. In particular,

one can use a Green's function, $G_i(\mathbf{x}, \mathbf{y})$, or impulse response function to relate the displacements of the overburden $u_i(\mathbf{x})$ to the fractional volume change, $\Delta v(\mathbf{y})$, within the reservoir

$$u_i(\boldsymbol{x}) = \int_V G_i(\mathbf{x}, \boldsymbol{y}) \Delta v(\boldsymbol{y}) d\boldsymbol{y} \tag{4-4}$$

where V is the reservoir volume (Rucci et al. 2013). The Green's function depends upon the elastic properties of the overburden and the effort required for its computation depends upon the complexity of this elastic model. There are analytic and semi-analytic techniques for homogeneous half-space and layered models, respectively, and numerical finite-difference and finite-element methods may be applied to fully three-dimensional models. The forward problem entails computing the displacements in the overburden given a distribution of volume change within the reservoir.

The inverse problem consists of using observations of the deformation of the overburden to estimate volume change within the reservoir. This is a much more difficult task because of the loss of resolution with depth, due to the smoothing effects of the Green's function in equation 4-4. For example, in Figure 4-13 we show the impulse response of a point volume change at the reservoir level. That is, we impose a volume change in a single grid block of the model and calculate the resulting range change on the surface. Due to the over 3 km depth of the reservoir the volume change spreads to an equivalent surface anomaly of over 3 km in diameter. This smoothing effect, along with any errors and contamination due to factors such as the imperfect removal of atmospheric effects can make the inverse problem unstable.

Figure 4-13. Impulse response due to a single grid block in the reservoir undergoing volume change
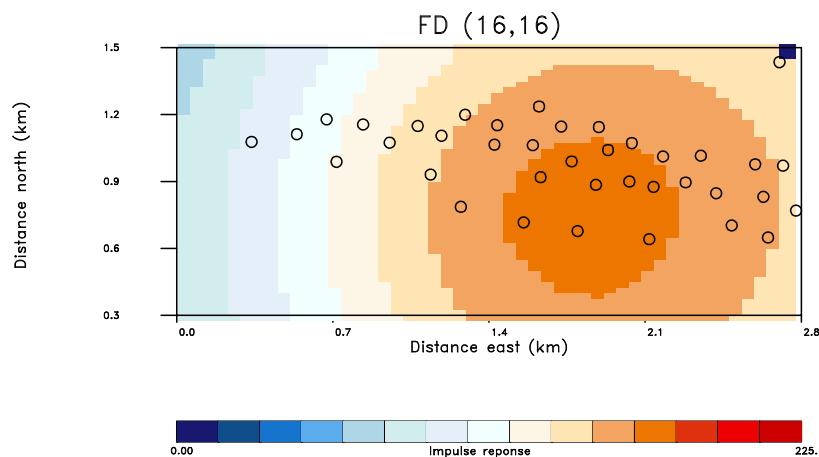
However, an inversion of the deformation can still be formulated, as a least squares minimization problem, and one can take advantage of the linearity of Equation 6-4 in solving for the spatial distribution of the reservoir volume change (Rucci et al. 2013). That is, we can relate the InSAR

range change, $r(\mathbf{x}_j, t)$, at a location $\mathbf{x}_j$ on the Earth's surface to the volume changes on rectangular grid blocks distributed over the reservoir volume:

$$r(\mathbf{x}_j, t) = \sum_{n=1}^{N} R_n(\mathbf{x}_j) a_n(t) = \mathbf{R}(\mathbf{x}_j) \cdot \mathbf{v}(t) \qquad (4\text{-}5)$$

where $R_n(x_j)$ is the integral of the projection of the Green's functions of the three displacement components along the look vector, $\mathbf{l}$, taken over the a grid block volume P_n:

$$R_n(\mathbf{x}_j) = \int_{P_n} l_i \cdot G_i(\mathbf{x}_j, y) dV \qquad (4\text{-}6)$$

Given a set of range change measurements, we can write the associated collection of linear constraints as a large system of equations for the reservoir volume changes. The inverse problem entails solving this linear system for the volume changes during each time interval. This is accomplished using a least squares approach where we minimize the sum of the squares of the residuals.

Due to the difficulty of the inverse problem it is important to devise appropriate regularization schemes to stabilize the process of estimating a solution. One particularly useful approach for volume changes that are induced by fluid extraction and injection into a reservoir is a regularization or penalty term that favors volume changes near known well locations (Vasco et al. 2010, Rucci et al. 2013, Vasco et al. 2019). Such a penalty term utilizes the fact that the effective pressure changes surrounding the well are driving the volume changes within the reservoir. Conventional regularization terms, such as model norm and roughness penalty functions, tend to produce excessively smooth solutions that exacerbate the loss of resolution with depth. Another way to regularize the inverse problem is via a model parameterization that accounts for known aspects of the source. For example, if the fluid volume changes are restricted to a specific formation with known boundaries one can incorporate that fact by restricting the source volume to that region. That is the case at Honor Rancho during normal operation, where the volume changes associated with the gas injection and production are restricted to the relatively thin reservoir region shown in Figure 4-12.

In order to stabilize the inverse problem at Honor Rancho, we introduce a term which penalizes volume changes that are far from the known well location. This penalty function is based upon the hypothesis that the reservoir volume changes are primarily driven by fluid pressure and temperature changes due to injection and that these changes are largest near the well itself. Therefore, we minimize the composite quadratic function in the volume changes $\mathbf{v}(t)$,

$$Q(\mathbf{v}) = (\mathbf{d} - \mathbf{Mv})^t \cdot (\mathbf{d} - \mathbf{Mv}) + \mathbf{v^t Dv} \qquad (4\text{-}7)$$

where $\mathbf{d}$ is the matrix of observed range changes, the data, $\mathbf{M}$ is a matrix with the j-th row given by $\mathbf{R}(\mathbf{x}_j)$, and a diagonal penalty matrix $\mathbf{D}$, that takes on large values for cells that are far from

the injection well. The necessary equations for the minimum of the quadratic function $Q(\mathbf{a})$, with respect to the components of the volume change vector $\mathbf{v}$, produces the desired linear system of equations. As an example of this approach, consider the range change that occurred between February 11, 2014 and March 4, 2014, plotted in Figure 4-14.

Figure 4-14. Range change between February 11th and March 4th, 2014 over Honor Rancho (negative range change is uplift)
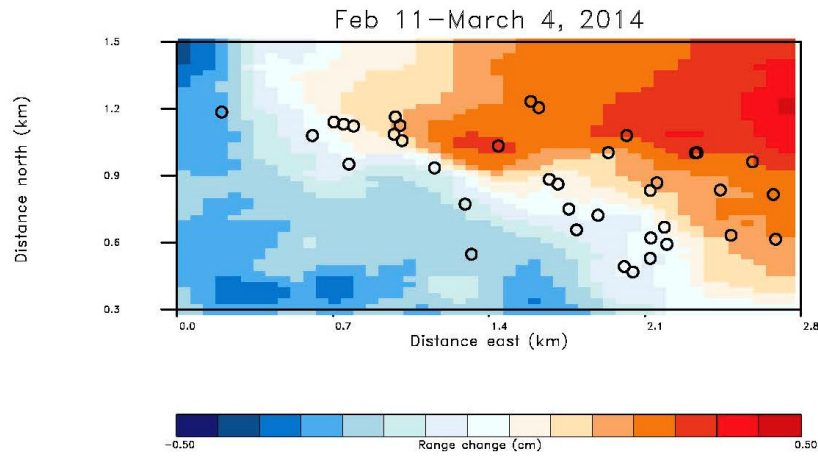
The open circles denote the well intersections with the reservoir.

Solving equation (4-7), using the well intersections shown in Figure 4-14, we can estimate the volume change in the reservoir that best explains the observed range change at the surface. The resulting estimate of volume change in the reservoir is shown in Figure 4-15.

Figure 4-15. Volume change obtained by an inversion of the range change data in Figure 4-14 (negative volume change means volume is decreasing)
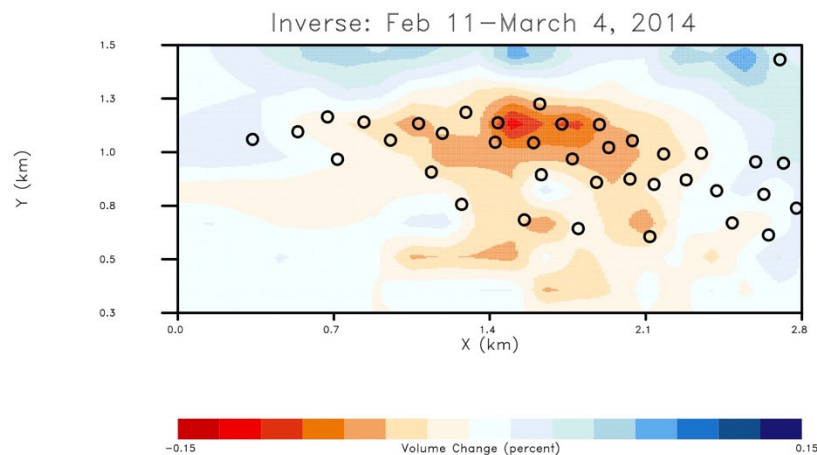
The solution in Figure 4-15 provides a model of volume change within the reservoir that best explains the observed range changes between February 11th and March 4th, 2014.

We can use the estimate of reservoir volume change and the observed range changes to identify anomalous events, i.e., time intervals during which it is difficult or impossible to fit the observed range changes with volume changes solely within the reservoir. Notice anomalous event just means an event with a large total residual. It does not mean that it signifies any particular event, but it suggests further examination. For example, the unusual event that was detected could be the interaction of regional tectonics or the operation of the reservoir, or water injection into the above storage zone. The essential idea is presented in Figure 4-16.

Figure 4-16. Calculation of InSAR residuals and the generation of a time series of total residuals as a function of calendar time

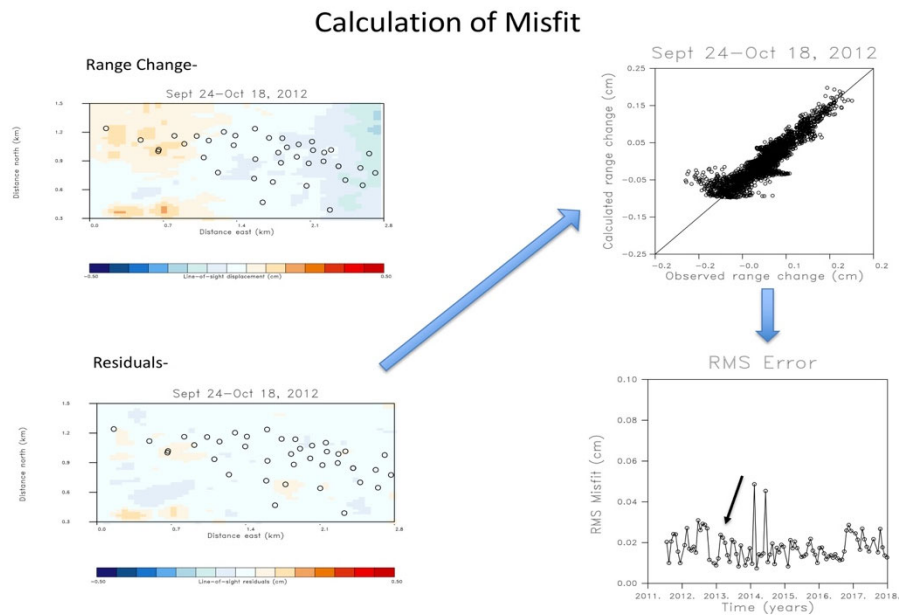The basic idea is to invert the InSAR observations for volume change in the reservoir and then consider the residuals, which are essentially the misfit to the observations. We can plot the sum of the misfits for each InSAR observation over the gas storage site to generate a total misfit. By examining the variation of these total misfits in time we can estimate the overall root-mean-squared misfit that is typically achieved for each inversion. This provides an estimate of the noise level in our data. Note that the noise level can include factors such as shallow hydrologic changes and atmospheric variations as well as random errors.

In order to test this approach, we applied it to some synthetic range changes generated by the numerical modeling code TOUGH-FLAC that is described in this 2nd annual report. Using reported injection rates, we modeled roughly 2000 days of injection and production into the gas storage facility. Two scenarios were considered: normal operation with no leak and anomalous behavior due to the occurrence of a leak at a depth above the reservoir. The RMS history for the situation in which there was no leak is shown in Figure 4-17. We observe that the RMS values randomly fluctuate around 0.01 mm RMS misfit.

51

Figure 4-17. RMS misfit as a function of calendar time for a simulation of the Honor Rancho gas storage facility
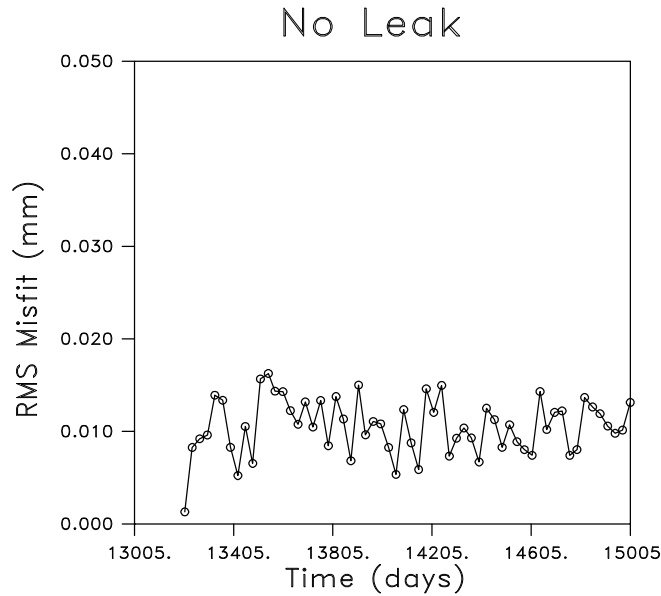
For the synthetic test data from the simulation in which there was a leak at a depth above the reservoir, we observed the same general variation initially, i.e., before the leak occurs. As before, the RMS misfit fluctuates randomly around a value of 0.1 mm. However, around 14000 days we observe a rapid increase in the level of misfit to values exceeding two times the previous RMS variation. The time at which we observe this increase coincides with the occurrence of the leak in the simulation.

Figure 4-18. RMS misfit history associated with a simulation in which a leak started at around 14000 days
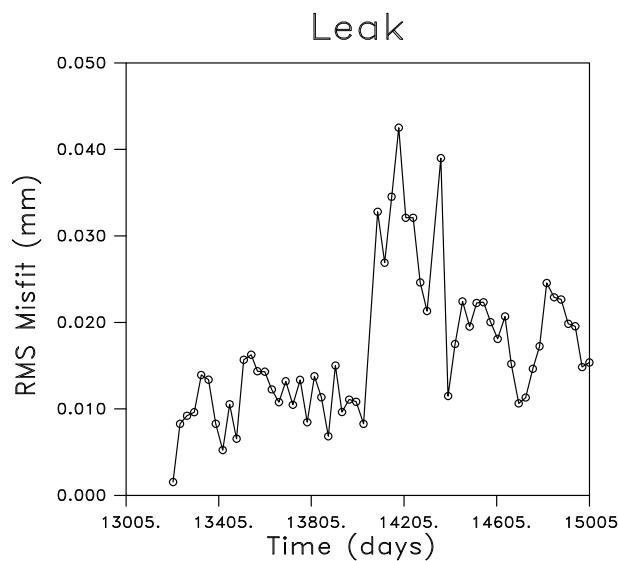
In addition to the synthetic test, we also applied the detection approach to our actual InSAR observations from the Honor Rancho gas storage site, such as that shown in Figure 4-14. The general characteristics of the resulting RMS variation are described in Figure 4-19.

Figure 4-19. Variation of RMS fit to the InSAR data from Honor Rancho
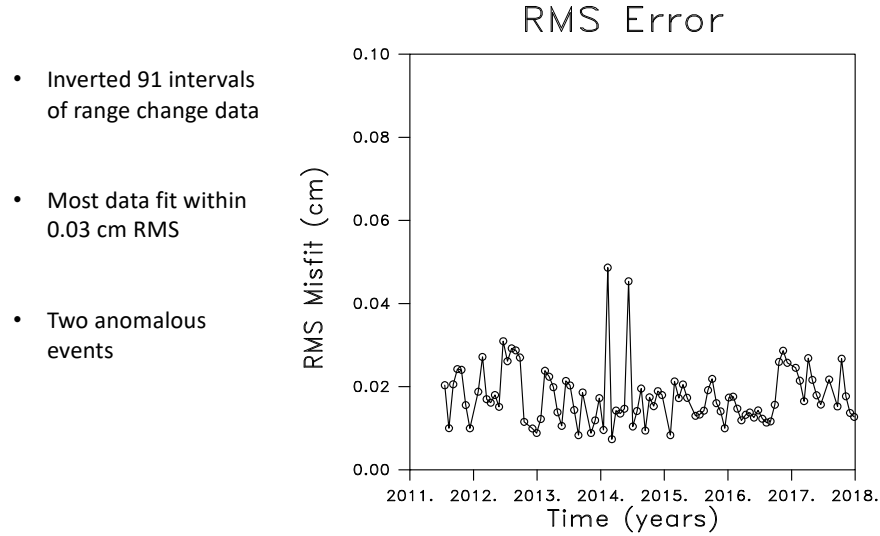
From the time series we observe general variations around 0.2-0.3 cm RMS variations with the exception of two anomalous time periods in 2014. This suggests that there are two time intervals that warrant further investigation. We can gain some insight into these two events if we examine the individual residuals plotted in map view (Figure 4-20).

Figure 4-20. Plot of the residuals associated with the first anomalous event plotted in a map view
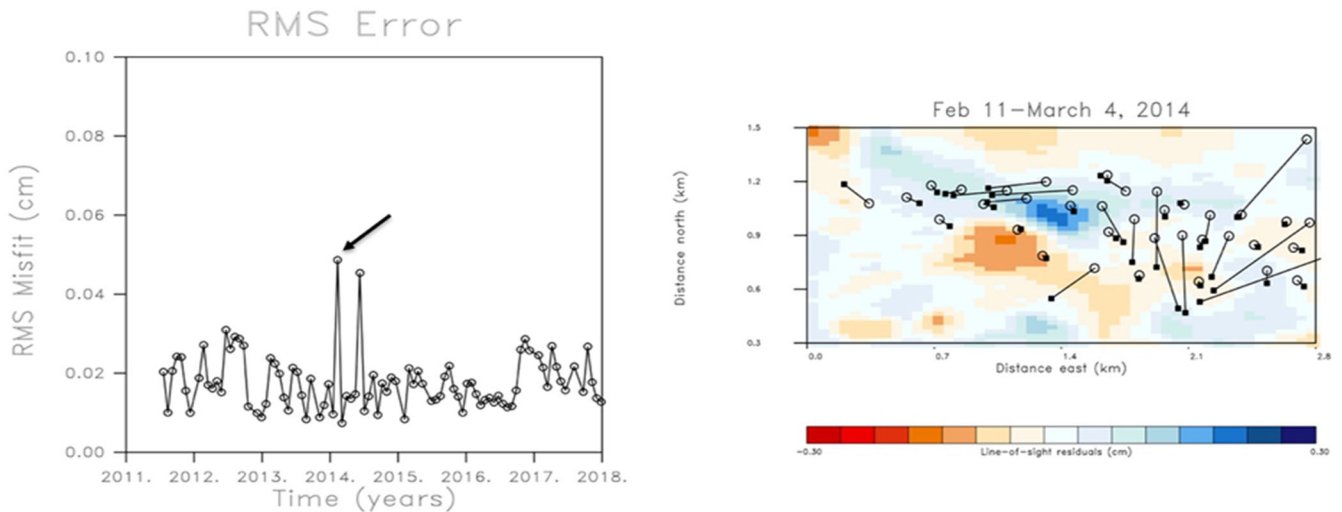
The largest residuals are concentrated near the center of the gas storage site and display a bi-modal pattern with a rapid transition between the positive and negative changes in the line of sight distance. The sharp change in sign indicates a source that is shallower than the gas

53

storage reservoir at 3-4 km depth. Interestingly, the residuals for the second anomalous event show a similar pattern but with the opposite sign (Figure 4-21), suggesting a reversal of the earlier movement.

Figure 4-21. Residuals associated with the second anomalous event (right panel) that is indicated by the arrow on the error plot to the left

These results show that InSAR observations may be used to monitor gas storage facilities and can provide evidence of anomalous behavior that may be used in an integrated system.

Summary

Interferometric Synthetic Aperture Radar observations provide a cost-effective method for monitoring an operating gas storage facility, even one as deep as Honor Rancho. While the surface deformation due to activities within the reservoir is small and can be accounted for through inversions for reservoir volume changes, processes above the reservoir such as slip on shallo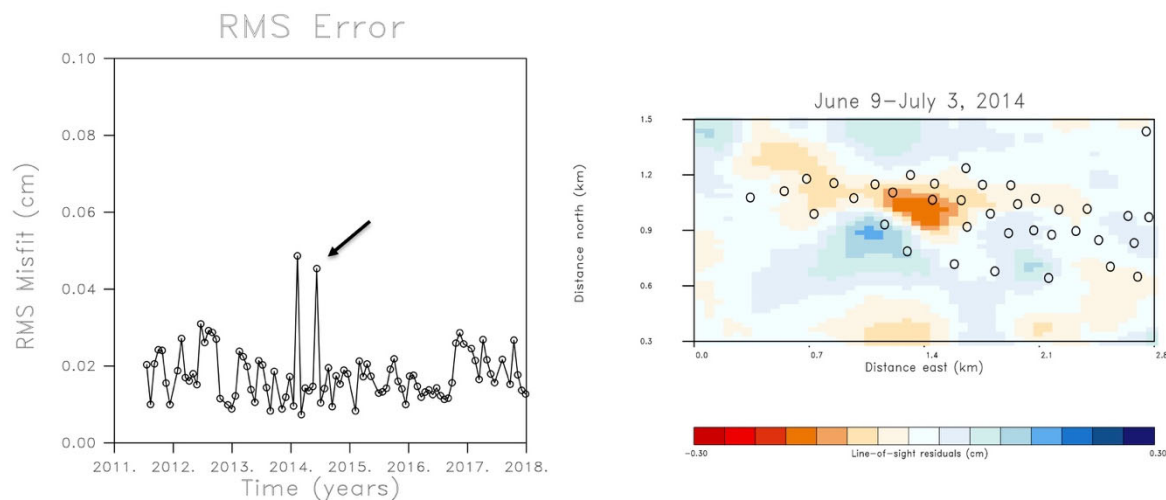w faults, leaks from wells above the reservoir, and landslides lead to larger signals that can be identified through their large residuals in a given observation interval. Synthetic testing indicates that well leaks of sufficient size can be identified due to anomalous residuals. Similarly, two events in the actual InSAR data from Honor Rancho indicated unusual surface deformation that warrants further investigation. Known activities, such as shallow water injection, need to be accounted for in order to improve the monitoring reliability and to reduce the possible misinterpretation of increased InSAR residuals. Anomalous events only signify a time interval where the residuals should be examined and interpreted. They do not necessarily signify an event within the gas storage facility on within the reservoir.

CHAPTER 5:
UAV Survey

Over the last several years, advanced gas leak detection systems have been developed and demonstrated to find leaks from UGS infrastructure (https://new.abb.com/products/measurement-products/analytical/laser-gas-analyzers/advanced-leak-detection). Among them, Unmanned Aerial Vehicle (UAV)/Drone technology has the advantage of flying over terrain that other technologies may not be able to access (e.g., sensitive habitat, steep topography, wetlands, etc.). UAV technologies are included in the IRMDSS as one of the surface monitoring technologies for leak detection.

Due to Covid-related site restrictions, the planned UAV drone survey at the Honor Rancho site could not be performed during the project period. Instead, an analogue site with a known leak source in Solano County, CA was used for monitoring demonstration purposes. ABB performed field surveys at the site. The goal of the surveys was to demonstrate UAV and other technologies as tools for gas leak detection. Below is a summary abstracted from the survey reports by ABB[1], [2].

Two visits were made to the same site for demonstrating methane detection and leak location capabilities of various technologies. The survey on the first visit on February 04, 2021 (referred to as the 2-4-2021 survey) was focused on an "artesian well" with a known low-level methane (CH_4) emission. The well is located on Nurse Slough Road, between several old oil and gas exploration fields (Kirby Hills, Kirby Hills North and Potrero Hills. Additional plugged dry oil/gas exploration wells are present along Nurse Slough Road (see Figure 5-1). Results from this visit suggested the presence of an additional previously unknown CH_4 source away from the road out in the marsh. As a result, ABB did a follow-up visit on March 23, 2021 (referred to as the 3-23-2021 survey) to survey around both the "artesian well" and the unknown marsh source.

In both visits, ABB surveyed the site with three technologies: MobileGuard (vehicle-based, mobile survey), HoverGuard (UAV-based, mobile survey) and MicroGuard (next generation handheld detection). Unlike systems that rely on path-averaged measurements (based on laser scattering or satellite), these systems record local (point) gas concentrations and wind velocity, thus resolving the plume and wind vectors as a function of time. From these multi-parameter measurements, the local flux rate at the source is estimated (from turbulent fluid dynamics models). Given the precision and time response of the technology, these systems (HoverGuard, MobileGuard, MicroGuard) resolve source volumetric flow rates far more accurately and sensitively than path-averaged approaches.

---

[1] ABB, XGUARD INVESTIGATION REPORT Nurse Slough Survey – 2021.02.04, Results Summary

[2] ABB, XGUARD INVESTIGATION REPORT Nurse Slough Survey – 2021.03.23, Results Summary

In the field demonstration, the source flow rate was also measured by tenting the source, blowing ambient air through the tent and measuring the increase in methane in the effluent as compared to ambient air flow. The measured methane flux is at 5.9 ± 0.5 ft^3/hr (CFH), which is used as the basis for quantification of the measurement error of the three technologies.

Figure 5-1. Survey location

HoverGuard Survey

In both visits, HoverGuard performed four separate flights of approximately 20 minutes each. Figure 5-2 shows HoverGuard making a close pass over the survey site.

Figure 5-2. Photo showing HoverGuard flying above the survey site

In the first survey, each of the flights used a different flight pattern, altitude, and speed. Flight 1 used a pattern that is suitable for variable wind, and guaranteed the source plume would be picked up at some point in the flight path; Flight 2 used a pattern that is suitable for consistent wind, and a site that is free-of-obstacles in the downwind area; Flight 3 repeated the Flight 2 pattern but at a higher altitude and at a higher speed; Flight 4 used a pattern useful for estimating source flow rates if propagation to a fixed measurement altitude cannot be guaranteed (usually because obstacles exist farther downwind). This variety of survey patterns was repeated in the second survey (3-23-2021 survey). Between the two visits, ABB implemented improvements to the emission rate estimation. Therefore, the 3-23-2021 HoverGuard rate estimates are more reliable compared to the ones from the 2-4-2021 survey.

Figure 5-3 shows the measured CH_4 concentrations from all four flights from the 2-4-2021 survey, indicating in addition to the source identified at the "artesian well", a potentially larger, previously unknown source exists farther out in the marsh. The separation between the indications from the "artesian well" and the newly identified source is noticeable and sufficient to conclude the CH_4 detected from the "artesian well" is not propagated from the newly identified larger source. Because the second source (out in the marsh) was not previously known, this field

demonstration provided the opportunity to demonstrate that the UAV can detect an unknown source, which is the main ultimate purpose of such surveys in the UGS monitoring context. During the second visit on March 23, as with the first 2-4-2021 survey, HoverGuard was able to detect the source at the "artesian well", along with the larger, previously unknown, emission source located farther out in the marsh on every flight. Additional detections of smaller, peripheral sources were also observed during the second visit. These smaller sources were more detectable during the second survey because of the lower winds on the day of the survey. By updating the aggregation algorithm, differentiability of sources was improved compared to the first reported results. Finally, a new method of visualizing the emission detections was developed that enhances to the ability to locate the source (Figure 5-4).

Figure 5-3. Plot of the measured CH$_4$ concentrations from all four flights in the 2-4-2021 survey
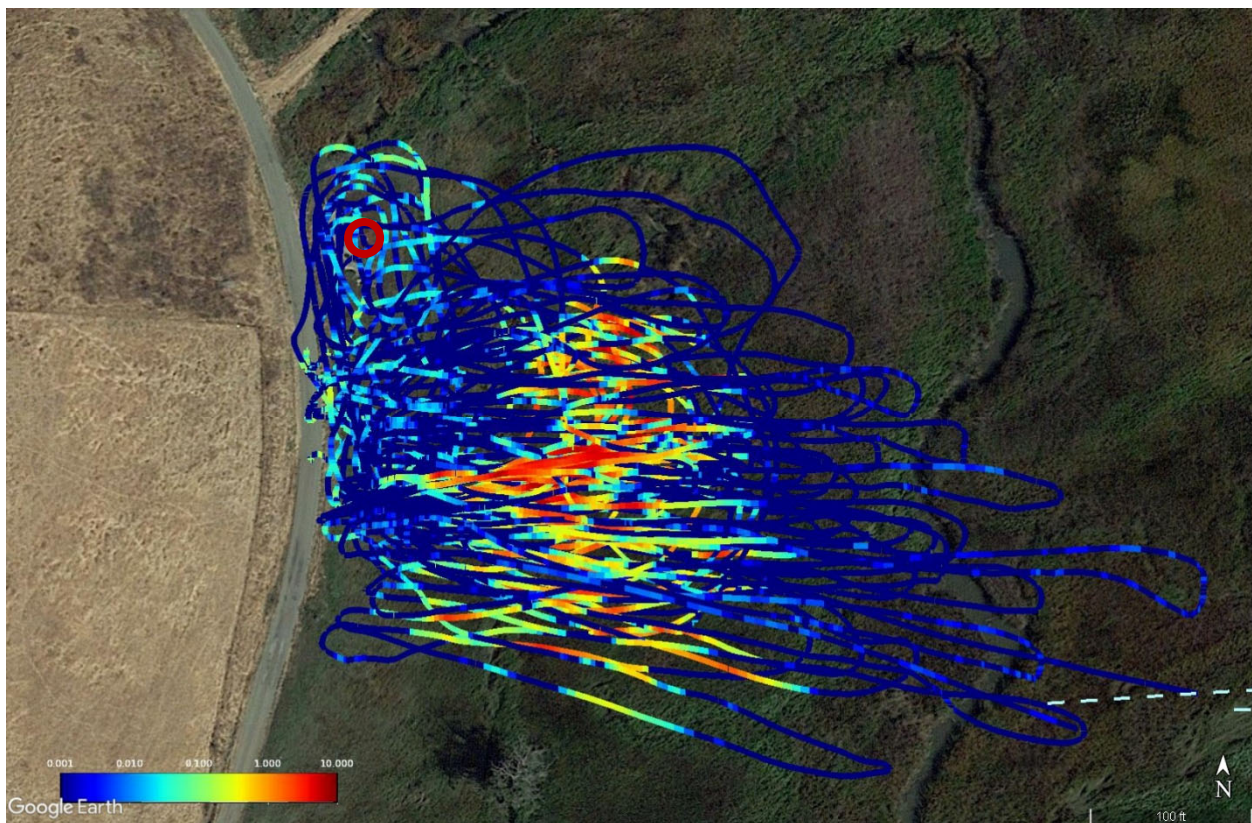
The 'artesian well' location is indicated by the red circle.

58

Figure 5-4. Detection density from all flights in the 3-23-2021 survey
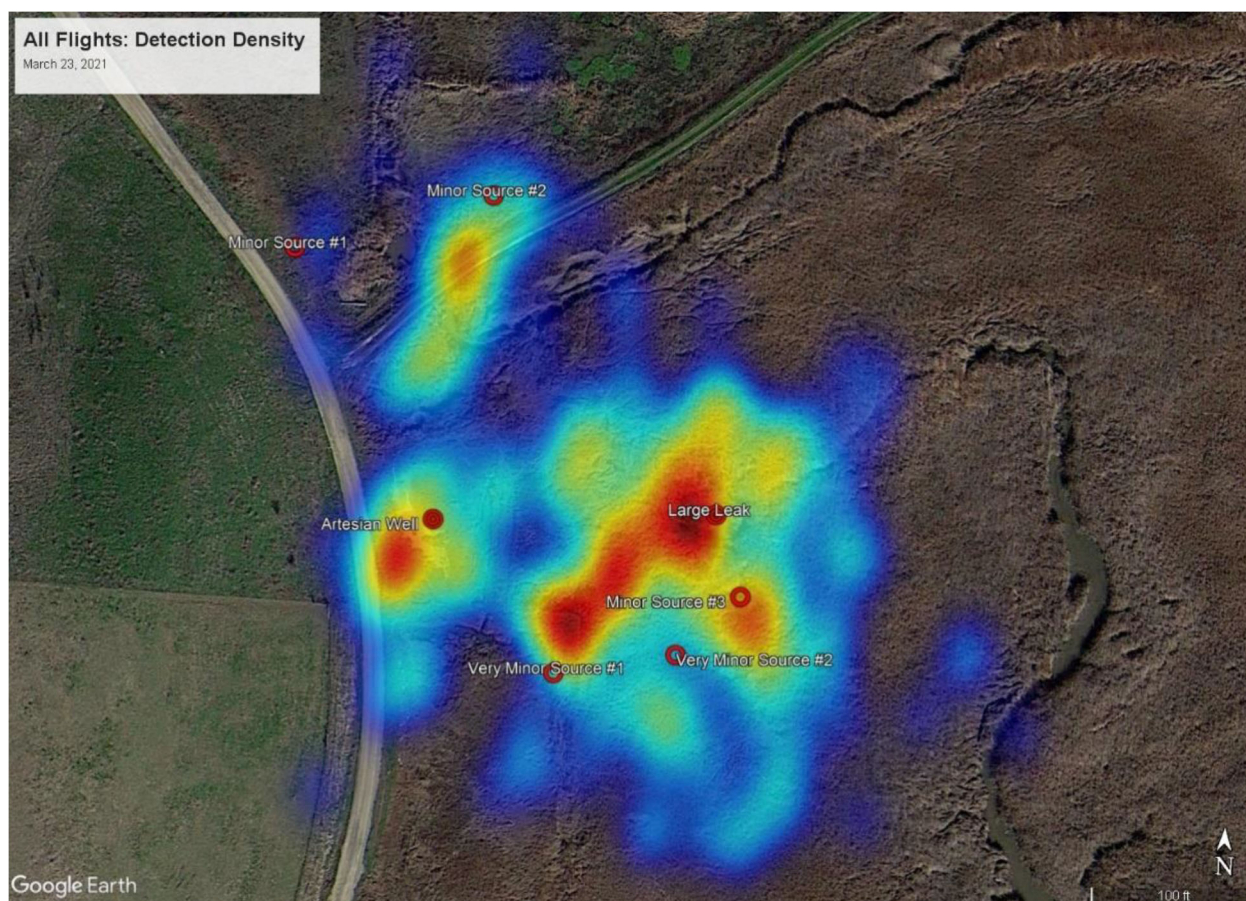
The various sources identified with the MicroGuard handheld sensor (discussed below) are clearly highlighted by the data collected by HoverGuard. Note this representation does not reflect emission severity.

MobileGuard Survey

ABB performed a vehicle-based, MobileGuard investigation in addition to the UAV-based inspection. Figure 5-5 shows the eight passes in the 2-4-2021 survey during which the vehicle was able to detect the nearest source (the "artesian well") because the generally northerly winds dispersed some of the emission to the roadway and the exceptional sensitivity of MobileGuard was able to identify the emission, estimate location, and estimate the flow rate. Two other sources were detected in that visit. One appears downwind of the well but still within the wind stream and is likely to be a repeated detection of the well; the other one appears upwind of the well and is likely to be biogenic.

The advantage of MobileGuard is that it measures both methane and ethane, which allows the system to speciate gas sources if the gas concentration is high enough, usually around 1 ppm for pipeline and/or stored natural gas sources that have ~3% ethane. In this case, MobileGuard failed to detect measurable ethane, likely indicating that the source gas has less than 3% ethane. In both surveys, no detectable ethane was present.

Figure 5-5. Measured methane from MobileGuard in the 2-4-2021 survey
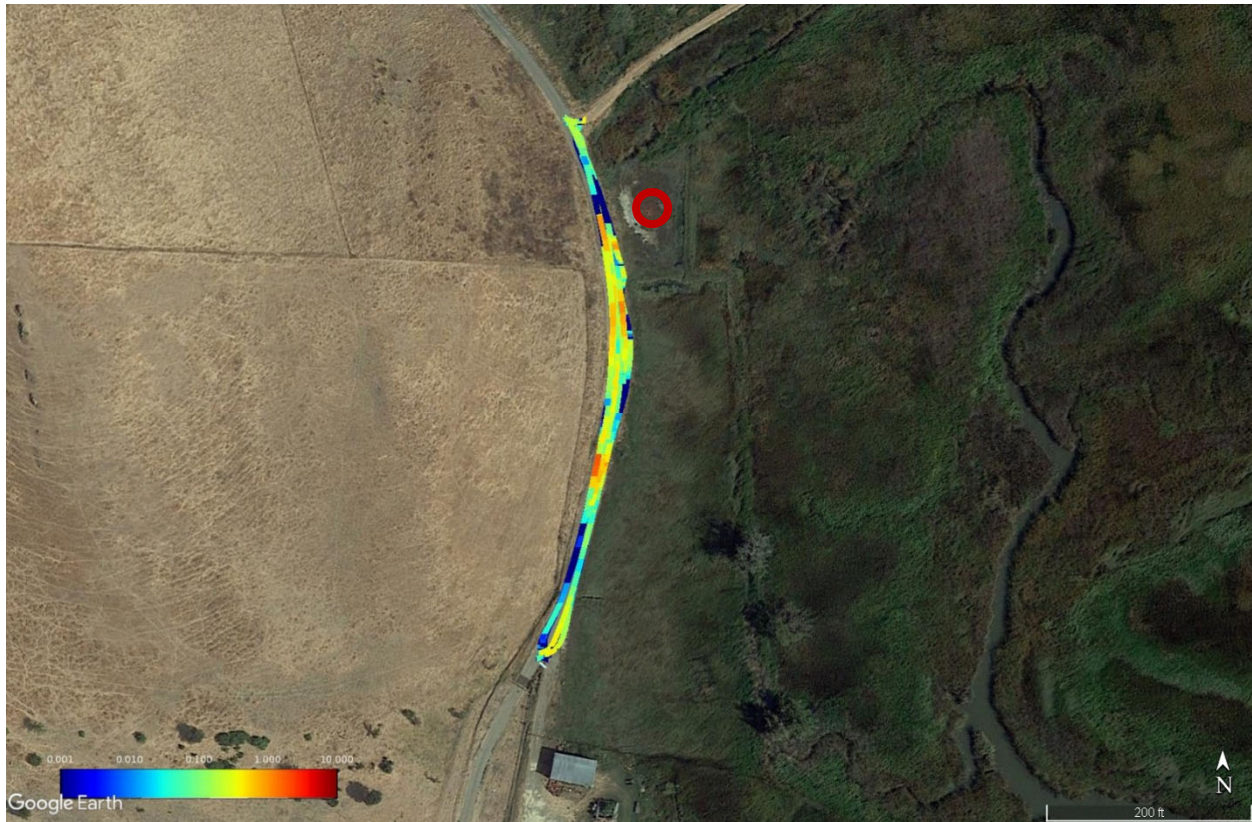
MicroGuard Survey

ABB conducted a pinpointing operation using the data collected from MobileGuard. Starting from the vehicle indication #1, ABB engineers used a proprietary search algorithm (carried out by a person on foot) to pinpoint the source location detected by the vehicle. This algorithm involves walking perpendicular to the prevailing wind (i.e., crosswind) while observing the instrument readings until excess methane (i.e., above local ambient level) is detected (typically 50-100 ppb above ambient) and then walking upwind until the excess methane is lost, then repeating crosswind walking to re-acquire the plume. This method results in extremely fast localization (less than 2 minutes under the conditions encountered during this survey). In the first visit, the MicroGuard focused on locating the source at the "artesian well". In the second visit, the investigation focused on locating the large unknown leak source that is farther out in the marsh and difficult to access.

Figure 5-6. Representation of the maximum measured methane by MicroGuard
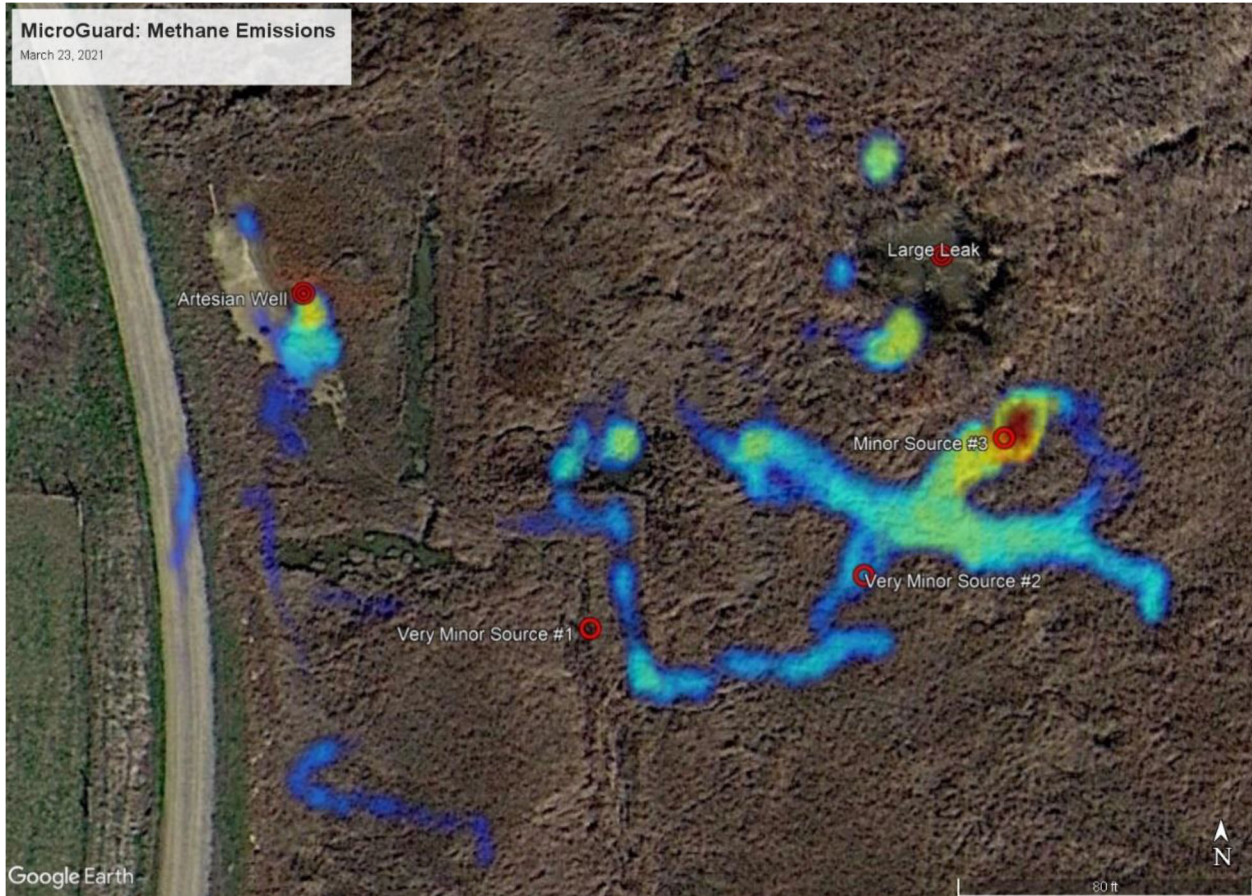
Areas downwind of the major sources have consistently elevated methane concentrations.

Results

The source location estimate error and leak rate estimate from HoverGuard and MobileGuard surveys are summarized in Table 5-1. Because the "artesian well" location is known, the error in positional estimation can be calculated. Both MobileGuard and HoverGuard were readily able to detect the source to within 35 and 27 meters and were able to accurately quantify the leak rate with a measurement error of 56% and 53%, respectively.

Table 5-1. Summary of survey results

System	Location accuracy	Leak rate Measurement	
	(m)	Volumetric flow (CFH)	Relative error
Flux chamber		5.9 ± 0.5	
HoverGuard	27.3 ± 6.3	9 ± 3.7	53%
MobileGuard	35	2.6 ± 1.8	56%

Summary

On February 4th, ABB surveyed an "artesian well" located in Solano County, CA off of Nurse Slough Rd with three different leak detection systems: HoverGuard (UAV-based), MobileGuard (vehicle-based) and MicroGuard (handheld). The gas flow rate out of the well was also measured using the chamber method to provide an actual leak rate value for comparison with the remote mobile measurements. Source localization for both HoverGuard and MobileGuard was within the error bounds and put users of MicroGuard in a position to rapidly pinpoint the source while walking. Estimated flow rates were determined by HoverGuard and MobileGuard and compared with the chamber flux measurement..In addition, the UAV-based gas leak detection system has the advantage of covering areas that may be inaccessible to conventional vehicles. Although unplanned, the demonstration field survey showed that the UAV can detect and approximately locate an upwind unknown leak. On March 23rd, ABB made a second visit to the site and pinpointed several likely biogenic sources using MicroGuard based on the initial estimated locations from the HoverGuard.

MobileGuard, the vehicle-based mobile survey has the advantage of measuring both methane and ethane, which allows the system to distinguish gas sources (e.g., natural biogenic from utility pipeline) if the gas concentration is high enough.

CHAPTER 6:
Summary and Conclusions

In this report we have documented data collected using advanced monitoring technologies for an integrated risk analysis for UGS facilities. Below we summarize all of the technologies demonstrated in this project.

DTS Monitoring

DTS data have been collected at the project well WEZU C2B at the Honor Rancho site both during gas injection and withdrawal, although the well is primarily used for injection. A temperature profile reflecting a cooling trend is expected during injection. During withdrawal, the temperature at the well bottom becomes cooler while the upper well becomes warmer. This is due to the temperature in the reservoir being lower than the temperature estimated using the geothermal gradient. The DTS profiles during normal operations provide a good baseline for identifying anomalies related to integrity issues. In addition, the DTS measurements provide the gas/liquid contact location in the annulus, which is an important piece of information for identifying integrity issues. We have not seen anomalies in the DTS data since we started to take DTS measurements. However, if an integrity issue were to arise, the vertical temperature measurements can be used with a combination of a wellbore flow model to identify potential leakage locations and quantify leakage flow rate for various leakage scenarios.

Using DTS data for well monitoring has the following advantages:

- data can be collected continuously and unsupervised;
- the gas-liquid interface level in the annulus can be read accurately each time an injection/withdrawal operation starts;
- changing conditions (in temperature or gas-liquid interface level) can provide an alarm of potential integrity issues in real-time;
- the monitoring data are easy to process and understand;
- the data can be combined with well models for further analysis;

We note that the DTS system entail higher per-well costs than periodic temperature logging.

DAS Monitoring

DAS data have also been collected at the project well WEZU C2B at the Honor Ranch site. In essence, DAS technology converts fiber-optic cables into massive arrays of seismic sensors that record the acoustic field at very high spatial and temporal resolution with minimal effort. Data can be recorded along the borehole at spatial density as high as 25 cm. Measurements can be made continuously in an unsupervised manner, as long as the instrument can be connected to a source of power and there is an adequate data storage system in place. These features make DAS a promising tool for long-term monitoring of UGS.

Our observations indicate that the analysis of acoustic noise recorded by DAS can provide critical information about changes occurring in the borehole at different stages of system

63

operation. In our analysis, we have been able to characterize these different stages, with the objective of setting background characteristics that describe the acoustic behavior of the system during normal operations. This knowledge will enable establishing what "normal behavior" is, so that anomalies are quickly identified and analyzed to search for malfunctions such as a leak. As stated in our introduction to this chapter, leaks are expected to generate characteristic acoustic signals that could be disentangled from the "normal" noise field.

With our data exploration approach, we have identified data attributes that can be quickly calculated for each DAS data file and can provide insights into spatial and temporal changes in the borehole. Such capability could be deployed in the IRMDSS approach. By continuously calculating the RMS amplitude and centroid frequency at each measurement point with a resolution of 30 s, we could identify anomalous behavior, release a warning and contrast the DAS observations with additional data streams (such as DTS, InSAR, etc.) to evaluate the potential for a hazard. On-going work in this framework regarding DAS will entail gaining a better understanding of the origin of the acoustic events observed while the well is flowing, and integrating the DAS capability into the IRMDSS system.

DAS data have shown to be a promising tool for gas leak detection. However, the technology is still in the research stage. The huge amount of data that flow from DAS monitoring systems remains a challenging problem. In addition, data processing and understanding need expert knowledge. The cost of DAS is high.

InSAR Monitoring

InSAR observations provide a cost-effective method for monitoring an operating gas storage facility, in addition to various routinely collected in-situ measurements, as well as the continuously collected DTS and DAS data demonstrated in this report. While the surface deformation due to activities within the reservoir is small and can be accounted for through inversions for reservoir volume changes, processes above the reservoir such as slip on shallow faults, leaks from wells above the reservoir, and landslides lead to larger signals that can be identified through their large residuals in a given observation interval. Synthetic testing indicates that well leaks of sufficient size can be identified due to anomalous residuals. Similarly, two events in the actual InSAR data from Honor Rancho indicated unusual surface deformation that warrants further investigation. Known activities, such as shallow water injection, need to be accounted for in order to improve the monitoring reliability and to reduce the possible misinterpretation of increased InSAR residuals. Anomalous events only signify a time interval where the residuals should be examined and interpreted. They do not necessarily signify an event within the gas storage facility on within the reservoir.

The main advantages of the InSAR data are: the technology is non-intrusive; and the cost is low. In order to make use of InSAR, the facility needs to have expertise in InSAR data analysis and inversion methods to translate surface deformation to subsurface (reservoir, overburden) movements.

UAV Survey

UAV surveys offer many advantages to other methods of gas leak detection. is the approach is non-intrusive and can be done as frequently as needed. Compared to vehicle-based and handheld CH_4 leak detection systems, the UAV-based gas leak detection system has the advantage of covering areas that may be inaccessible to conventional vehicles. The leak flow rate can be estimated accurately. When the UAV is combined with handheld device, the leak source can be pinpointed quickly. The algorithm/analysis in the demonstrated system allows monitoring, detection, and leak-locating to be carried out by field technicians.

GLOSSARY

Term/Acronym	Definition
CFH	Cubic feet per hour
DAS	Distributed acoustic sensing
DTS	Distributed temperature sensing
GPS	Global Positioning System
InSAR	Interferometric Synthetic Aperture Radar
IRMDSS	Integrated Risk Management and Decision-Support System
UAS	Unmanned Aerial System
UAV	Unmanned Aerial Vehicle
UGS	Underground natural Gas Storage

REFERENCES

Authur, Daniel. 2016. Application of well integrity methods for gas storage wells. 23rd IPEC Conference. https://cese.utulsa.edu/wp-content/uploads/2017/06/2016-IPEC-APPLICATION-OF-WELL-INTEGRITY-METHODS-FOR-GAS-STORAGE-WELLS.pdf.

Berardino, P., Fornaro, G., Lanari, R., 2002. A new algorithm for surface deformation monitoring based on small baseline differential SAR interfereograms. *IEEE transactions on Geoscience and Remote Sensing,* **40** (11), 2375-2383.

Ferretti, A., Prati, C. and Rocca, F. (2001). Permanent Scatterers in SAR Interferometry, *IEEE Transactions on Geoscience and Remote Sensing*, **39**(1), 8 -20.

Ferretti, A. (2014). Satellite InSAR Data – Reservoir Monitoring from Space. EAGE Publications.

Hartog, A. H., Rao, Y.-J., Ran, Z.-L., Gong, Y., Güemes, A., & Sierra Perez, J. (2017). An Introduction to Distributed Optical Fibre Sensors. (A. H. Hartog, Ed.). Boca Raton, Florida: Taylor and Francis Group.

Hooper, A. (2008). A multi-temporal InSAR method incorporating both persistent scatterer and small baseline approaches, *Geophysical Research Letters*, **35**, L16302, 1-5.

Lanari, R., Mora, O., Manunta, M., Mallorqui, J. J., Berardino, P, and Sansosti, E. (2004). A small baseline approach for investigating deformations on full-resolution differential SAR interferograms, IEEE Transactions on Geoscience and Remote Sensing, 42, 1377-1386

Lindsey, N.J., Rademacher, H., Ajo-Franklin, J.B. (2019) On the Broadband Instrument Response of Fiber-Optic DAS Arrays, Journal of Geophysical Research: Solid Earth, 125(2).

Maslennikova Y.S., Bochkarev, V.V., Savinkov, A.V., Davydov, D.A. (2012) Spectral Noise Logging Data Processing Technology, Proceedings of the SPE Russian Oil and Gas Exporation and Production Technical Conference and Exhibition, 16-18 October, Moscow, Russia.

MDA, (2013). *Playa del Rey, California InSAR Ground Deformation Monitoring Interim Report* H., Ref: RV-14524, MDA Spatial Services, Ontario, Canada

Rucci, A., Vasco, D. W. and Novali, F. (2013). Monitoring the geologic storage of carbon dioxide using multicomponent SAR interferometry. *Geophysical Journal International*, **193**(1), 197-208

Samsonov, S., d'Oreye, N. (2012). Multidimensional time series analysis of ground deformation from multiple InSAR data sets applied to Virunga Volcanic Province. *Geophysical Journal International*, **191**, 1095-1108, http://dx.doi.org/10.1111/j.1365-246X.2012.05669.x.

Samsonov S., van der Koij M. and Tiampo, K., 2011. A simultaneous inversion for deformation rates and topographic errors of DInSAR data utilizing linear least square inversion technique, *Computers & Geosciences*, 37 (8), 1083-1091

Teatini, P, Castelletto, N., Ferronato, M., Gambolati, G., Janna, C., Cairo, E, Marzorati, D., Colombo, D., Ferretti, A., Bagliani, A., and Bottazzi, F., (2011), Geomechanical response to seasonal gas storage in depleted reservoirs: A case study in the Po River basin, Italy, *Journal of Geophysical Research*, **116**, 1-21

Vasco, D. W., Rucci, A., Ferretti, A., Novali, F., Bissell, R. C., Ringrose, P. S., Mathieson, A. S., and Wright, I. W., (2010), Satellite-based measurements of surface deformation reveal fluid

flow associated with the geological storage of carbon dioxide, *Geophysical Research Letters*, **37**, L03303, 1-5, doi:10.1029/2009GL041544.

Vasco, D. W., Farr, T. G., Jeanne, P., Doughty, C., and Nico, P. (2019). Satellite-based monitoring of groundwater depletion in California's Central Valley, *Nature Scientific Reports*, **9**, 16043, doi.org/10.1038/s41598-019-52371-7.

Zeng, F. H., Zhao, G., Zhu, L.J., 2012. Detecting CO2 leakage in vertical wellbore through temperature logging. Fuel 94, 374-385.

Zhang, Y. Jung, Y., Freifeld, Y., and Finsterle, S.. (2018). Using distributed temperature sensing to detect CO2 leakage along the injection well casing, *Int. J. Greenhouse Gas Control*, doi.: 10.1016/j.ijggc.2018.04.011.